Interactions of cytosolic tails in the Jen1 carboxylate transporter are critical for trafficking and transport activity

Cláudia Barata-Antunes[1,2*], Gabriel Talaia[1,3*], George Broutzakis[4], David Ribas[1], Pieter De Beule[5], Margarida Casal[1,2], Christopher J. Stefan[6], George Diallinas[4,7*] and Sandra Paiva[1,2*]

[1]Centre of Molecular and Environmental Biology, Department of Biology, University of Minho, Braga, Portugal

[2]Institute of Science and Innovation for Bio-Sustainability (IB-S), University of Minho, Portugal

[3]Department of Cell Biology, Yale University School of Medicine, New Haven, CT, USA

[4]Department of Biology, National and Kapodistrian University of Athens, Panepistimiopolis 15784, Athens, Greece.

[5]International Iberian Nanotechnology Laboratory, Avenida Mestre José Veiga s/n, Braga, Portugal

[6]Institute of Molecular Biology and Biotechnology, Foundation for Research and Technology, Heraklion, Greece

*The authors contributed equally to the work

Correspondence: George Diallinas: diallina@biol.uoa.gr and Sandra Paiva: spaiva@bio.uminho.pt

Abstract

Plasma membrane (PM) transporters of the major facilitator superfamily (MFS) are essential for cell metabolism, growth and response to stress or drugs. In *Saccharomyces cerevisiae,* Jen1 is a monocarboxylate/H^+ symporter that provides a model to dissect the molecular details underlying cellular expression, transport mechanism and turnover of MFS transporters. Here, we present evidence revealing

novel roles of the cytosolic N- and C- termini of Jen1 in its biogenesis, PM stability and transport activity, using functional analyses of Jen1 truncations and chimeric constructs with UapA, an endocytosis-insensitive transporter of *Aspergillus nidulans*. Our results show that both N- and C-termini are critical for Jen1 trafficking to the PM, transport activity and endocytosis. Importantly, we provide evidence that Jen1 N- and C- termini undergo transport-dependent dynamic intra-molecular interactions, which affect the transport activity and turnover of Jen1. Our results support an emerging concept where the cytoplasmic termini of PM transporters control transporter cell-surface stability and function through flexible intra-molecular interactions with each other. These findings may be extended to other MFS members to understand conserved and evolving mechanisms underlying transporter structure-function relationships.

Key words: Major facilitator superfamily (MFS); transporters; monocarboxylic acids; endocytosis; arrestins; cytosolic termini; sorting; turnover; substrate specificity; ubiquitylation.

Introduction

Eukaryotic plasma membrane (PM) transporters play essential roles in cell nutrition, signalling, and responses to stress conditions and drugs. Consequently, transporter malfunction has an impact in many aspects of human cell biology and leads to several pathologies, including neurological and cardiovascular disorders, as well as diabetes and cancer (Bowton et al., 2014; Gonzalez-Menendez et al., 2017; Morgan et al., 2011; Sakrikar et al., 2012; Scheffner and Kumar, 2014). Given their importance in sensing the environment and maintaining cellular homeostasis, transporter function depends on complex and fine regulatory mechanisms. However, our knowledge of PM transporter regulation is not yet complete, especially regarding roles of transporter cytoplasmic termini.

Endocytic internalization is a major regulatory mechanism of PM transporters extensively studied in the model fungi *Saccharomyces cerevisiae* and *Aspergillus nidulans*, in response to physiological or stress signals, followed by either their vacuolar degradation or recycling back to the PM (for recent reviews see (Barata-

Antunes et al., 2021; Diallinas and Martzoukou, 2019; Kahlhofer et al., 2020). Endocytic internalization of fungal PM transporters requires ubiquitylation at their C- or N-terminal cytosolic regions by HECT-type E3 ubiquitin ligases (including Rsp5 in *S. cerevisiae* or HulA in *A. nidulans*), which are recruited by adaptor proteins named α-arrestins (Becuwe and Léon, 2014; Becuwe et al., 2012a; Gournas et al., 2010; Karachaliou et al., 2013; Lin et al., 2008; Merhi and Andre, 2012; Nikko and Pelham, 2009; Talaia et al., 2017). In *S. cerevisiae*, fourteen α-arrestins have been identified, named Arts (Art1-10), Buls (Bul1-3) and Spo23, which all possess PY motif(s) that may interact with WW domains of the Rsp5 Ub ligase, mediating membrane protein turnover (Becuwe et al., 2012a; Lin et al., 2008; Nikko and Pelham, 2009; Novoselova et al., 2012; O'Donnell et al., 2010; Yashiroda et al., 1996). *A. nidulans* possesses 10 α-arrestins, including ArtA and PalF, which control transporter downregulation and pH sensing, respectively (Barata-Antunes et al., 2021; Karachaliou et al., 2013), while in mammals six α-arrestins have been identified, named ARRDC proteins (Alvarez, 2008; Rauch and Martin-Serrano, 2011), but much less is known regarding their role, specifically on transporter cellular expression.

Previous studies in *S. cerevisiae* have proposed that α-arrestins recognize the exposed cytoplasmic N- and C-termini of nutrient transporters (Crapeau et al., 2014; Ghaddar et al., 2014; Gournas et al., 2017; Guiney et al., 2016; Keener and Babst, 2013; Lin et al., 2008; Marchal et al., 1998; Marchal et al., 2000; Merhi et al., 2011). These segments contain specific α-arrestin interacting motifs and ubiquitin target sites. For example, the N-terminus of the general amino acid transporter Gap1 contains a potential Bul1/2 α-arrestin interacting motif and two Ub target sites that are required for nitrogen-elicited endocytosis of Gap1 (Ghaddar et al., 2014; Merhi et al., 2011). Additionally, under stress conditions, Bul1/2, in combination with Art3/Art6, promotes Gap1 ubiquitylation and downregulation *via* the Gap1 C-terminus (Crapeau et al., 2014). In these cases, it is thought that conformational changes during substrate transport makes the N-terminus more accessible to α-arrestins (Ghaddar et al., 2014; Gournas et al., 2017).

In the filamentous fungus *A. nidulans,* a C-terminus region of the uric acid transporter UapA is essential for ArtA-mediated ubiquitylation, endocytosis, and vacuolar degradation in response to ammonium or excess of substrate (Gournas et al., 2010; Karachaliou et al., 2013). Also, in *A. nidulans,* the FurE nucleobase-allantoin transporter has been shown to possess elements in its N- and C-terminus

that are critical for endocytosis and, surprisingly, for substrate specificity. In this case, the authors provided evidence that the N- and the C-terminus interact physically and promote proper transporter function and turnover (Papadaki et al., 2017; Papadaki et al., 2019). Whether long-range regulatory effects of cytosolic N- and C-termini extend to transporters other than Fur-like proteins or other members of the amino acid–polyamine–organocation (APC) superfamily (Mikros and Diallinas, 2019), remains to be formally shown. These findings raise new questions regarding conserved, intrinsic roles of the cytoplasmic termini of transporters, including APC and MFS members.

Specifically, and importantly, do transporter termini contribute to transporter function and regulation in ways that are distinct from their known roles in transporter endocytosis and downregulation?

Here, we address roles of the cytosolic terminal regions of Jen1, a yeast monocarboxylate/H^+ symporter (lactate and pyruvate being its major substrates) that represents the ubiquitous and largest transporter family, the so-called major facilitator superfamily (MFS). By functionally analysing N- and C-terminally truncated versions of Jen1, we provide compelling evidence that both cytosolic termini of Jen1 are crucial for the biogenesis, transport kinetics, and turnover of Jen1. Using quantitative bi-fluorescence complementation (BiFC) assays, we present further evidence that the two Jen1 termini interact dynamically in a transport-activity dependent manner, which ultimately regulates Jen1 cell-surface expression and activity. Our findings support the idea that cytosolic termini of MFS transporters provide important multi-functional roles, which should be examined as a general emerging concept in transporter regulation.

Results

Rationale for constructing Jen1 truncations

Jen1 has been used extensively as a model cargo to dissect mechanisms of regulated transporter internalization. Jen1 ubiquitylation, endocytosis, and vacuolar degradation are regulated by two α-arrestins (Rod1 and Bul1), in response to distinct stimuli (Becuwe et al., 2012b; Fujita et al., 2018; Hovsepian et al., 2018; Talaia et al., 2017). Recently, a C-terminal region of Jen1 was reported to be involved in Rod1-

mediated endocytosis of the transporter, triggered by glucose (Fujita et al., 2018). However, roles of the Jen1 N- and C-termini in PM targeting, transport activity, and endocytic downregulation are incompletely understood.

To further elucidate roles of the cytosolic termini of Jen1 in its regulation, we employed specific N- or C-terminus truncations of Jen1. Prior to these constructions, it was essential to define the limits of the N- and C-terminus of Jen1 based on available structural information. At first, the selection of the number of residues corresponding to the cytosolic N- and C-terminus portions of Jen1, which lacks an experimentally defined structure, was based on standard topology predictions and homology threading modelling (detailed in **Table S1).** These predictions were used to construct five separate truncated versions of Jen1 expressed from a low-copy centromeric plasmid in a *S. cerevisiae jen1*Δ strain. All Jen1 versions were expressed as C-terminal *GFP* fusion proteins (see Materials and methods). Two truncations lacked 133 or 94 N-terminal amino acids (Jen1ΔNT133 and Jen1ΔNT94), two lacked the 64 or 33 C-terminal amino acids (Jen1ΔCT64 and Jen1ΔCT33), and the fifth lacked both the 94 N-terminal and the 33 C-terminal amino acids (Jen1ΔNT94ΔCT33) (**Figure 1A** and **B**). We also employed the AlphaFold tool for 3D protein structure prediction (alphafold.ebi.ac.uk) to visualize the predicted structure of Jen1 including the N- and C-termini. **Figure 1C** shows the predicted structure of Jen1, highlighting the truncated regions in the cytosolic termini. This approach indicated that the large terminal truncations (Jen1ΔNT133 and Jen1ΔCT62) remove helical segments that may be extensions of TMS1 or TMS12, respectively, necessary for Jen1 function. Consistent with this notion, subsequent analyses showed that the Jen1ΔNT133 and Jen1ΔCT62 truncated proteins are non-functional (**Figure S1** and **Figure 2**).

Specific N- and C-terminal truncations of Jen1 reveal an important role of cytosolic termini in PM localization, stability and transport kinetics

We analysed the growth and ^{14}C-lactic acid transport activity of strains expressing either full-length or truncated Jen1 forms (**Figure 2A** and **2B**). The two larger terminal deletions of Jen1 (Jen1ΔNT133 and Jen1ΔCT62) abolished Jen1-dependent growth on lactate, as sole carbon source, (**Figure 2A**) and led to loss of Jen1 transport activity (**Figure 2B**), resembling the negative control lacking Jen1

(*jen1*Δ cells carrying the empty p416-GPD plasmid). In contrast, the three shorter truncated versions of Jen1 (Jen1ΔNT94, Jen1ΔCT33 and Jen1ΔNT94ΔCT33) were able to confer growth on lactate and ^{14}C-lactic acid transport activity similar to Jen1 wild-type (WT) control cells (**Figure 2A** and **2B**). The recorded transport capacities in the mutants were confirmed by measurements of external medium alkalinisation that occurs upon Jen1-mediated lactate uptake (Talaia et al., 2017), as only full-length Jen1, Jen1ΔNT94, Jen1ΔCT33, and Jen1ΔNT94ΔCT33 led to an increase in the pH of the medium (**Figure S1A**).

The subcellular localization of the truncated Jen1 proteins (**Figure 2C** and **S1B**) was monitored upon switch to lactate that promotes Jen1 localization to the PM (Lac 4 h) and after sequential addition of glucose (Lac 4 h + Gluc 2 h) that leads to endocytic turnover. As expected, stable localization of wild-type Jen1 to the PM was observed upon growth in lactate (Lac 4 h), while endocytosis and sorting to vacuoles for degradation was observed 2 h after the addition of glucose (Lac 4 h + Gluc 2 h). The Jen1ΔNT133 and Jen1ΔCT62 proteins bearing large truncations showed significant retention in the ER, revealed by fluorescent labelling of nuclear ER (nER) rings as well as discontinuous fluorescence at the cell periphery that is typical of cortical ER (cER) in yeast (**Figure 2C**). Co-staining with CMAC indicated that the intracellular rings do not correspond to vacuoles (**Figure S1B**). In the case of Jen1ΔCT62, retention in the ER was confirmed by expression in a *S. cerevisiae* strain lacking six ER-PM tethering proteins. In this strain (named Δ*tether*), contacts between the cER and the PM are significantly decreased, allowing ER-resident proteins to be unambiguously distinguished from those localized to the PM (Manford et al., 2012). In this strain, an ER-resident marker (DsRed-HDEL), clearly co-localized with Jen1ΔCT62-GFP, but not with the functional Jen1ΔCT33-GFP protein (**Figure S2A**). Jen1ΔNT133 and Jen1ΔCT62 may be misfolded and retained in the ER which could explain, at least in part, why these proteins are non-functional. The cytosolic termini of some transporters contain ER export signals, such as di-acidic, hydrophobic and aromatic variable short sequences (for a review see (Mikros and Diallinas, 2019)). Interestingly, the longer N- and C-termini of Jen1 harbour similar motifs that may be necessary for COPII-mediated ER exit or for proper folding (^{1126}NPIPE^{133} and ^{577}EYE^{579}, respectively; see **Figure S2B**). These regions are worthy to be studied by mutational analysis, in the future.

The functional truncated Jen1 proteins also displayed interesting localization patterns. Jen1ΔNT94-GFP, although fully functional as demonstrated by growth tests and lactate transport assays (**Figure 2A** and **2B**), displayed a clear decrease in PM localization and a corresponding increase in vacuole localization even in the absence of glucose (Lac 4 h) (**Figure 2C**, **Figure S1B**). This suggests that Jen1ΔNT94, even upon constitutive expression, undergoes very rapid constitutive internalization from the PM and sorting to the vacuole for degradation. In contrast, Jen1ΔCT33-GFP localized to the PM with no indication of ER retention after 4 h in lactate (**Figure 2C**). Notably, Jen1ΔCT33-GFP displayed strong fluorescence at the PM, consistently stronger than wild-type Jen1-GFP, suggesting that this truncation stabilizes the transporter. Jen1ΔCT33-GFP also showed reduced vacuole localization upon glucose addition, when compared to wild-type Jen1-GFP (**Figure 2C** and **S1B**). These initial results suggested that loss of N-terminal domain may expose residues in the C-terminal domain involved in α-arrestin dependent endocytosis. In support of this model, the doubly truncated Jen1ΔNT94ΔCT33 version stably localized to the PM, and it was more resistant to glucose-induced endocytosis as compared to both full-length Jen1 and Jen1ΔCT33 (**Figures 2C** and **S1B**). These data were supported by the quantification of the ratio of the fluorescence at the plasma membrane over the total fluorescence at the time point Lac 4 h + Gluc 2 h (**Figure 2D**). The ratio obtained for the Jen1ΔNT94ΔCT33 was the highest (0.51), followed by the one determined for the Jen1ΔCT33 (0.40). As expected, the ratio for the Jen1ΔNT94 (0.29) was similar to the wild-type Jen1 (0.26). This suggests that loss of the last 33 residues of Jen1 is not only epistatic to the instability conferred by deleting the N-terminal 94 residues, but also points to the idea that the two termini of Jen1 might interact functionally.

To better understand the effect of deleting the terminal segments on Jen1 function, we investigated whether functional truncations (Jen1ΔNT94, Jen1ΔCT33 and Jen1ΔNT94ΔCT33) affect the transport kinetics of lactate, via direct measurements of lactic acid transport (**Figure 3**). All Jen1 truncations tested, including Jen1ΔNT94, which proved to be unstable at the PM, displayed higher substrate affinities (lower K_m) compared to wild-type Jen1. Notably, deleting the C-terminal region in Jen1ΔCT33 resulted in a 10-fold increase in substrate affinity. The doubly truncated Jen1ΔNT94ΔCT33 version and Jen1ΔNT94 also had 2.5 to 3-fold increased affinity for lactate. Thus, transport kinetics of Jen1 truncations revealed

that specific segments of the N- and C- termini are critical for substrate binding and transport dynamics, in addition to their role in PM sorting, PM stability, and regulated endocytosis. These results unmask previously unappreciated functions of the N- and C-termini.

Glucose-triggered endocytic turnover of Jen1 involves complex interactions of Rod1 and Bul1/2 with the Jen1 N- and C-termini

Glucose-induced Jen1 internalization has been reported to require both Rod1 and Bul1/2 arrestins (Becuwe et al., 2012b; Hovsepian et al., 2018), suggesting that multiple α-arrestins may recruit the ubiquitylation machinery necessary for Jen1 endocytosis. A glucose-responsive degron recognized by Rod1 has been recently identified in the C-terminus of Jen1 (Fujita et al., 2018). However, no binding motif has been identified for the Bul1 and Bul2 arrestin paralogs. Moreover, it is not known whether Rod1 interacts with other regions in Jen1 including the N-terminus.

We investigated the localization and relative PM levels of the functional Jen1 proteins in wild-type cells (*ROD1*$^{+}$ *BUL1/2*$^{+}$) and in strains lacking the Rod1 and Bul1/2 arrestin proteins (*rod1*Δ, *bul1*Δ*bul2*Δ or *rod1*Δ*bul1*Δ*bul2*Δ) (**Figures 4** and **S3**). In these assays, GFP-tagged Jen1 versions were expressed from the *GAL1* promoter (Gal 5 h), and then glucose was added for 2 or 4 h to repress expression and trigger Jen1 internalization and subsequent degradation in the vacuole (see Materials and methods). At the times indicated, cells were collected, visualized by fluorescence microscopy (**Figures 4A-D**) and relative levels at the PM (as a fraction of the total GFP signal) were determined (**Figure 4E**).

Results obtained in the wild-type background (*ROD1*$^{+}$ *BUL1/2*$^{+}$) showed that full-length Jen1 is internalized and targeted to the vacuole after glucose addition (**Figure 4A**). This was confirmed by Jen1 co-localization with CMAC, a known vacuolar marker (**Figure S3A).** Internalization of full-length Jen1 was delayed in a strain lacking Rod1, but was localized to the vacuole in *bul1*Δ*bul2*Δ cells following addition of glucose similar to wild-type cells (**Figures 4B-C** and **4E;** see also **S3B-C**). Internalization of full-length Jen1 was further impaired in *rod1*Δ*bul1*Δ*bul2*Δ triple deletion mutant cells, as compared to *rod1*Δ single mutant cells (**Figures 4D** and **4E;** see also **S3D**). This was further supported by western-blot analyses that revealed, that, upon 4 h of glucose, steady state levels of Jen1 remained relatively high when

Rod1 was absent (i.e. *rod1*Δ and *rod1*Δ*bul1*Δ*bul2*Δ) (**Figure S4B**, **S4D** and **S4E**). Notice also that in *rod1*Δ there is the relative decrease in Jen1 levels between 2 and 4 h of glucose addition (**Figure S4B** and **S4E**), suggesting that absence of Rod1 does not fully rescue Jen1 from turnover in agreement with localization results shown in **Figure 4A-E**. Overall, the results suggest that Rod1 is the principal arrestin that mediates glucose-induced Jen1 endocytosis, although it does not totally rescue Jen1 form sorting to the vacuole, while Bul1/2 do not seem to be required for endocytosis, under the experimental conditions used. Interestingly, however, glucose-triggered Jen1 endocytosis was significantly blocked in the triple mutant cells (**Figure 4E**), revealing that the Bul1/2 proteins may have a compensatory role upon loss of Rod1, in line with previous reports (Becuwe et al., 2012b; Hovsepian et al., 2018). The additive effect of deleting Rod1 and Bul1/2 might further suggest that these arrestins compete for a common cytoplasmic target in Jen1 and that Rod1 has a higher affinity for this target compared to Bul1/2.

We carried out similar experiments using the functional truncated versions of Jen1. Quantitative fluorescence microscopy demonstrated that Jen1ΔNT94 underwent glucose-induced internalization and delivery to vacuoles in wild-type cells (*ROD1*$^{+}$ *BUL1/2*$^{+}$) (**Figure 4A, 4E** and **S3**). In contrast, glucose-induced internalization of Jen1ΔNT94 was significantly impaired in *rod1*Δ mutant cells (**Figure 4B, 4E** and **S3**), consistent with previous work suggesting that Rod1 binds an endocytic signal in the Jen1 C-terminus (Fujita et al., 2018). Glucose-induced Jen1ΔNT94 internalization was also impaired in *bul1*Δ*bul2*Δ double mutant cells and *rod1*Δ*bul1*Δ*bul2*Δ triple mutant cells, although to a lesser extent than *rod1*Δ mutant cells (**Figure 4E**). Western-blot analyses showed that the deletion of the first 94 residues led to a very unstable Jen1 protein in all genetic backgrounds, especially in the presence of glucose (**Figure S4A-D** and **S4E**). Notice for example that although we were able to detect PM associated fluorescence of Jen1ΔNT94 in *rod1*Δ*bul1*Δ*bul2*Δ (**Figure 4E**), we could not detect the intact protein in the relative western experiment (**Figure S5D**). The reason for this is not clear, but it might be related to the fact that cells observed under the microscope and those used to extract proteins are necessarily treated differently. Still however, we could detect stabilization of the Jen1ΔNT94 protein in *rod1*Δ, in line with the idea that Rod1 exerts its activity via the C-terminus of Jen1.

As expected, glucose-induced internalization of Jen1ΔCT33 was impaired as compared to full-length Jen1 in wild-type cells (**Figure 4A**, **4E**). Unexpectedly however, glucose-induced Jen1ΔCT33 internalization was further impaired in *rod1*Δ mutant cells as compared to wild-type control cells (**Figure 4E**). Glucose-induced Jen1ΔCT33 internalization was also impaired in *bul1*Δ*bul2*Δ and *rod1*Δ*bul1*Δ*bul2*Δ mutant cells as compared to wild-type cells (**Figure 4E**). The Jen1ΔNT94ΔCT33 protein displayed significant defects in glucose-induced internalization in wild-type, *rod1*Δ, *bul1*Δ*bul2*Δ, and *rod1*Δ*bul1*Δ*bul2*Δ cells alike (**Figure 4E**).

Western blot analyses confirmed that Jen1ΔCT33 and Jen1ΔNT94ΔCT33 were very stable Jen1 versions. Notice also that the doubly truncated version Jen1ΔNT94ΔCT33 was more stable than Jen1ΔCT33 in the wild type or *rod1Δ* backgrounds, but not in Δ*bul1*Δ*bul2*Δ or *rod1*Δ*bul1*Δ*bul2*Δ, further revealing that Bul1/2 act via the N-terminus of Jen1 (**Figure S4B** and **S4E**). Taken together, these results demonstrate that the Jen1 N- and C-termini are both involved in Jen1 downregulation and that they undergo complex interactions with both Rod1 and Bul1/2 arrestins.

Overall, the findings thus far revealed that the Jen1 N- and C-termini function in Jen1 biogenesis in the ER, substrate binding affinity and transport at the PM, as well as regulated endocytosis. The data also indicated that both of the Jen1 termini undergo complex interactions with alpha-arrestin family members. Next, we addressed whether the N- and C-termini are sufficient for endocytic uptake. We also sought to monitor dynamic interactions between the N- and C-termini during substrate binding and transport activity.

The C-terminus of Jen1 is sufficient for promoting glucose-elicited turnover of UapA via interaction with Rod1

To further investigate the functional role of Jen1 termini, we employed the construction and functional analysis of chimeric transporters based on the UapA transporter from *A. nidulans.* These chimeras were designed to carry the cytosolic termini of Jen1 fused with UapA. UapA is an extensively studied uric acid-xanthine/H^+ symporter (for a review see (Diallinas, 2016)), which is regulated by ammonium or substrate-elicited endocytosis in *A. nidulans*. However, upon functional expression in *S. cerevisiae*, it does not respond to endocytosis and,

instead, remains stable at the PM (Leung et al., 2010). Thus, UapA provides an appropriate molecular marker for investigating, via domain swap experiments, the potential, context-independent, functional role of *cis*-acting elements present in Jen1 N- or C-terminal regions. Chimeras of UapA/Jen1 were constructed as illustrated in **Figure 5A**. Briefly, the intact UapA coding sequence was fused with amino acid segments 1-94 (i.e., NT94) or/and 584-616 (i.e., CT33) of Jen1 termini, resulting in the chimeric transporters named UapA/Jen1NT94, UapA/Jen1CT33 and UapA/Jen1NT94-CT33. For details of strains see Materials and methods. We analysed these chimeras by uptake transport assays (**Figure 5B**), epifluorescence microscopy and western blotting, in different *S. cerevisiae* strains (**Figure 6** and **7**).

UapA, UapA/Jen1NT94, UapA/Jen1CT33 and UapA/Jen1NT94-CT33 conferred saturable ^{3}H-xanthine import (**Figure 5B**), which strongly suggested that UapA and the chimeras are all translocated to the PM and are transport-active. In fact, UapA and the single chimeras UapA/Jen1NT94 and UapA/Jen1CT33 showed very similar K_m and V_{max} values. The K_m values measured were also similar to the native K_m of UapA measured in *A. nidulans* (7.0 ± 2.0 μM (Alguel et al., 2016)). The double chimera UapA/Jen1NT94-CT33 showed reduced rate of transport, as the relevant K_m and V_{max} values were increased and reduced, respectively, an indication that this chimera might be partially misfolded when expressed in yeast (**Figure 5B**).

The subcellular localization of wild-type UapA and the three chimeras (UapA/Jen1NT94, UapA/Jen1CT33 and UapA/Jen1NT94-CT33) was followed in a standard wild-type *S. cerevisiae* carrying a *jen1* deletion (*jen1*Δ). UapA and the single chimeras UapA/Jen1NT94 and UapA/Jen1CT33 showed significant PM localization, concomitant with partial retention in the ER, most evident in the case of UapA/Jen1NT94 (**Figure 6A**, upper row). The double chimera UapA/Jen1NT94-CT33 seemed to be massively retained in ER-like cytosolic structures. The ability of UapA/Jen1NT94 and UapA/Jen1CT33 chimeras to translocate to the PM was also confirmed in the strain lacking the ER-PM tethering proteins (**Figure S5**), where the PM resident proteins can be unambiguously distinguished from those localized to the ER (Manford et al., 2012). Overall, these findings were in accordance with uptake assays, showing that the single UapA/Jen1 chimeras embedded in the PM are also transport-competent (**Figure 5B**).

After having established that UapA and UapA-Jen1 single chimeras are translocated to the yeast PM and function with proper kinetics, we followed their response to glucose-triggered endocytosis **(Figure 6A**, middle and lower rows). In the presence of glucose, the localization profile of UapA and UapA/Jen1NT94 was similar with that obtained without glucose, suggesting that the relevant proteins are insensitive to glucose-triggered endocytosis. Notably, however, the presence of glucose elicited detectable endocytic turnover of UapA/Jen1CT33. This was evident after 2 h in the presence of glucose, where fluorescent vacuoles co-stained with CMAC appear and the PM-associated fluorescence signal is reduced. Thus, the CT33 region of Jen1 seems to confer, glucose-dependent turnover of UapA.

We also analysed the localization of UapA and UapA-Jen1 chimeras in *rod1*Δ and *bul1*Δ*bul2*Δ strains, in the absence or presence of glucose. In both tested genetic backgrounds wild-type UapA was translocated to the PM with some evidence of moderate ER-retention irrespectively of the presence of glucose, as probably expected (**Figure 7 A-B**). UapA/Jen1CT33, the chimera shown to respond to endocytosis by glucose in a wild-type background (*ROD1*$^{+}$*BUL1/2*$^{+}$) (see **Figure 6**), when expressed in *rod1*Δ strain, was localized to the PM, irrespectively of the presence or absence of glucose (**Figure 7 A-B)** and did not co-localize with vacuoles. In contrast, UapA/Jen1CT33 PM localization in *bul1*Δ*bul2*Δ is affected by the presence of glucose similar to the wild-type background. This suggested that glucose-triggered endocytic turnover of this chimera is Rod1-dependent and Bul1/2-independent. The localization of UapA/Jen1NT94 was not affected in *rod1*Δ and *bul1*Δ*bul2*Δ strains, or by the absence or presence of glucose (data not shown).

To better understand the response of UapA/Jen1CT33 to glucose-elicited, apparently Rod1-dependent endocytosis, we measured the steady state protein levels of wild-type UapA and UapA/Jen1CT33 by western blotting. As shown in **Figure 7C-D**, UapA/Jen1CT33 protein levels were significantly reduced in a Rod1-dependent manner in the presence of glucose, unlike those of wild-type UapA. These results suggest that the C-terminus of Jen1 is sufficient to promote glucose-elicited, Rod1-dependent, turnover of UapA, in a context-independent manner. In addition, our findings confirm that Bul1/2 plays no role in glucose-elicited endocytosis of UapA/Jen1CT33.

Dynamic transport-dependent interaction of N- and C-termini of Jen1

Our results strongly suggested that N- and C- termini of Jen1 contain elements critical for biogenesis, function and turnover of Jen1. Most notably, the effects of Jen1 cytosolic termini on Jen1 functional expression proved additive and complex. This was highlighted by the significant stabilization of Jen1, when truncated at both termini, in comparison to what was found for the singly truncated versions. These findings also suggested that the termini of Jen1 might interact with each other during the conformational changes accompanying transport activity, which is also associated to endocytic turnover. To further investigate this issue, we used a Bimolecular fluorescence (BiFC) assay, based on reconstitution of YFP florescence when the two parts of the split YFP epitope are fused in the two termini of Jen1 (YFPn-Jen1-YFPc). Given that reconstitution of YFP might in principle also occur in case Jen1 dimerizes, we also constructed a strain co-expressing the two parts of the split YFP epitope fused in distinct Jen1 molecules (i.e., Jen1-YFPn or Jen1-YFPc). These strains and relative controls (i.e., strains expressing Jen1-YFPn or Jen1-YFPc or co-expressing both) were used to investigate whether YFP is reconstituted in *cis* via interaction of the Jen1 termini, or/and in *trans* via dimerization of Jen1 molecules (for details of constructs see Material and methods). **Figure 8A** shows that strong, PM-associated, reconstitution of YFP fluorescence occurs solely when the split epitope parts are fused with the termini of Jen1, whereas no fluorescent signal was obtained when these are fused in different Jen1 molecules. This result not only strongly suggests that the two termini of Jen1 come in close contact when attached in the same Jen1 molecule, but also points against tight dimerization of distinct Jen1 molecules, at least under the conditions tested. To address further the mechanism by which the two termini of Jen1 come into contact, we repeated our assay in the presence of substrate. **Figure 8B** (left panel) shows that the presence of lactic acid reduced significantly the YFP fluorescence signal over time, but had no effect on the strength of fluorescent signal coming from Jen1-GFP. Noticeably, the relative strength of reconstituted YFP fluorescence in the presence of lactic acid fluctuated overtime. These findings show that stable reconstitution of YFP is transport activity dependent, further suggesting that conformational movements accompanying translocation of the substrate might affect the positioning of the two termini in the outward- and inward- facing topologies of Jen1 (see **Figure 8C**). The transport-dependent interaction of N- and C-termini of Jen1 is very similar to what has been

observed in FurE, which is a member of the evolutionary, structurally and functionally distinct NCS1/APC superfamily (Papadaki et al., 2019).

Discussion

In the present work, we investigated possible functional roles of the terminal cytosolic segments of the Jen1 monocarboxylate transporter in *S. cerevisiae.* Our first approach consisted in designing, genetically constructing and functionally analysing truncated versions of *GFP*-tagged Jen1, lacking parts of their cytosolic termini, expressed in wild-type or mutant *S. cerevisiae* strains lacking the arrestins Rod1 or Bul1/2. Our functional analyses included Jen1-mediated growth tests on lactic acid, or effect on external pH, direct measurements of Jen1 transport kinetics using radiolabelled lactic acid, *in vivo* imaging of subcellular localization, and western blot measurements of protein steady state levels of the truncated Jen1 versions. These constructs were expressed under induction conditions and in response to physiological signals triggering Jen1 endocytosis (i.e., glucose). Subsequently, we generated and analysed functional chimeric transporters made of UapA, a heterologous nucleobase-allantoin transporter of *A. nidulans,* fused with the terminal regions of Jen1.

Deleting the entire Jen1 terminal regions, which correspond to 133 N-terminal or 62 C-terminal amino acids, as defined by *in silico* predictions, led to non-functional Jen1 versions, which in most cases were associated with significant cellular mislocalization, mostly ER-retention. Alphafold 3D prediction of Jen1 structure justified this result as these deletions removed part of the transmembrane segments of Jen1. We thus proceeded by analysing shorter truncations, as those deleting the 94 N-terminal or/and the 33 C-terminal amino acids. Notice that similar truncated versions of Jen1 have been previously analysed (Fujita et al., 2018), which allowed direct comparison of relevant results (see later). The shorter Jen1 truncations were proved to be functional based on growth tests and other functional assays, similarly to what has been previously reported in (Fujita et al., 2018). Based on these Jen1 truncations and relative chimeras with UapA, we came to the following primary observations.

Role of the C-terminus. Jen1ΔCT33 is a stable version of Jen1, in all conditions tested, showing also increased capacity of lactate transport, not only because of its higher concentration in the PM, but also due to 10-fold increased affinity for its substrate. This suggests that the segment of the C-terminal 33 amino acids deleted in the truncated version, contains not only a degron, as reported by Fujita et al. (Fujita et al., 2018), but also a functional motif that seems to affect the mechanism of transport of Jen1 in an 'allosteric' manner. This conclusion was based on the fact that the cytosolic C-terminus, as predicted by Alphafold, is distant from the proposed substrate translocation trajectory (Soares-Silva et al., 2011). A similar situation of regulation of transport kinetics by genetic modifications of the cytosolic C-terminus has only been reported in the case of FurE, an *A. nidulans* nucleobase-allantoin transporter (Papadaki et al., 2017; Papadaki et al., 2019). Additionally, we presented evidence that the C-terminal 33 amino acid segment of Jen1 contains the major Rod1 interacting motif, as also reported in Fujita et al. (Fujita et al., 2018), given that its deletion (i.e., ΔCT33) mimicked the absence of glucose-triggered endocytosis of Jen1, observed in a *rod1* null mutant. Furthermore, in the absence of Bul1/2, full endocytosis was observed in wild-type Jen1 and Jen1ΔNT94, but not in Jen1ΔCT33. Finally, we showed that the interaction of Rod1 with the 33 amino acid C-terminal segment of Jen1 is very probably direct and context-independent, because its transfer to the endocytosis-insensitive UapA proved sufficient to promote Rod1-dependent downregulation, in the presence of glucose. Overall, our results concerning the C-terminal part of Jen1 confirm the conclusions presented in Fujita et al (2018), but further reveal two novel and important properties of this part of the transporter. First, the C-terminus of Jen1 regulates the transport mechanism from a distance, and second, Rod1 recognizes a motif in the C-terminus of Jen1 without the involvement of other regions of the transporter. To our knowledge, there is no other report showing a context-independent interaction of a transporter motif with α-arrestins.

Role of the N-terminus. Jen1ΔNT94 was shown to be normally produced at basal levels, but proved to be a rather unstable version of Jen1, exhibiting rapid turnover upon further induction. Thus, the N-terminal 94 residues segment of Jen1 should include elements critical for post-translational stability, evident upon translocation to the PM. Interestingly, Jen1ΔNT94 showed moderately altered transport kinetics (e.g., 2.5-fold increased substrate affinity), which points to a

positive ‘distant’ effect on the transport mechanism, albeit weaker than that of the C-terminal segment. Notably also, the N-terminal part proved critical for endocytic downregulation in response to glucose, because when *ROD1* gene was knocked-out or the C-terminus of Jen1 was deleted (i.e., no Rod1 binding), the presence of the N-terminus conferred partial endocytosis, while its absence led to an increased stability. Our data further support the conclusion that glucose triggered endocytosis of Jen1 can also be exerted via Bul1/2 binding to the N-terminal segment, as endocytosis without the C-terminal region (Jen1ΔCT33) or without an active *ROD1*, depends solely on Bul1/2.

Dynamic interactions of the N- and C-termini of Jen1. A clear conclusion concerning the termini of Jen1 is that both are needed for maximal glucose-triggered endocytosis of Jen1, with the N-terminus interacting with Bul1/2 and the C-terminus with Rod1. The interaction of Rod1 with the C-terminus seems to result in stronger Jen1 endocytosis when Bul1/2 interaction with the N-terminus is blocked. The interaction of Bul1/2 with the N-terminus confers only partial endocytosis, when Rod1 interaction with the C-terminus is genetically abolished. In our opinion, the most interesting novel finding of this work is the evidence supporting the hypothesis that the two Jen1 termini co-operate in regulating the stability and function of Jen1. A first genetic indication supporting this idea came from the doubly truncated Jen1 version, which showed exceptional new properties, other than those of the singly truncated mutants and the wild-type Jen1. Specifically, Jen1ΔCT33ΔNT94 shows very high PM stability, under all conditions and genetic backgrounds tested. Thus, the doubly truncated Jen1 version is practically a ‘new’ monocarboxylate transporter that is endocytosis resistant and that has a 3-fold increased substrate affinity relative to the wild-type Jen1.

To address the molecular basis underlying the additive functional roles of Jen1 termini, we employed a BiFC assay, which showed a dynamic and transport-dependent interaction of the two termini of Jen1. Using the same assay, we also obtained strong evidence that Jen1 does not form dimers, at least in the conditions tested, which proved fortuitous for more rigorously interpreting the positive BiFC signals obtained when the two parts of split YFP were cloned in the same Jen1 molecule. The only other previously reported case where BiFC assays showed that cytosolic termini interact to control the function and turnover of a transporter, is that of FurE in *A. nidulans* (Papadaki et al., 2017; Papadaki et al., 2019). In this case,

interactions of the two termini affected the stability, trafficking, function and endocytosis of FurE and, surprisingly, substrate specificity. Preliminary Molecular Dynamic analysis has provided some hints on how cytosolic termini might have affected FurE functioning from a distance by modifying the opening and closing of outer and inner gates of the transporter (Papadaki et al., 2019). In the present work, Jen1 truncations did not seem to affect substrate specificity, but interestingly, all functional Jen1 truncations showed increased (2.5 to 10.0-fold) affinities for lactic acid transport, despite retaining wild-type V_{max} values (see **Figure 3**). The alteration in K_m values reveals a modification in the capacity of Jen1 truncations to bind native substrates. In other words, similar to FurE, changes on the cytosolic termini of Jen1, distantly positioned from the substrate binding site, affect the mechanism of substrate selection and transport. How this is achieved, in the case of Jen1, remains elusive but constitutes an interesting point to be addressed in the future.

The present work on Jen1 shows that transporter cytosolic termini can be exploited to rationally modify transporter function, which will be valuable, not only for addressing basic mechanisms of solute transport, but also for serving as tools in biotechnological applications ((Kim et al., 2014; Knychala et al., 2022; Tanaka et al., 2017), for a review see (Barata-Antunes et al., 2021)). The generality of this concept is supported by the work on FurE and Jen1, representing the two major transport superfamilies, APC and MFS, but also several other reports directly or indirectly supporting the emergence of transporter termini as important functional elements (Mikros and Diallinas, 2019).

Supporting Information

This article contains supporting information.

Materials and Methods

Yeast strains and Growth conditions

All the yeast strains used in this work are listed in **Table S2**. The strains *jen1*Δ, *rod1*Δ, *bul1*Δ*bul2*Δ and *rod1*Δ*bul1*Δ*bul2*Δ were derived from the 23344c wild type strain (Laboratory collection). For BiFC analysis, a *jen1*Δ strain derived from W303-

1A was used (Laboratory collection). Yeast cells were grown in a synthetic minimal medium with 0.67 % (w/v) yeast nitrogen base (Difco), supplemented to meet the auxotrophic requirements (YNB medium) or in yeast extract (1 %, w/v) and peptone (1 %, w/v) (YP medium). Solid media was prepared adding agar (2 % w/v) to the respective liquid media. Carbon sources utilized were glucose (2 %, w/v), lactic acid (0.5 %, v/v, pH 5.0), galactose (2 %, w/v) or glycerol (3 %, v/v). Growth was carried out at 30 °C. Cultures were harvested during the mid-log phase of growth. Glucose-grown cells were, then, centrifuged, washed twice in deionized water and cultivated into a fresh YNB medium with lactic acid (incubation time is indicated). For induction conditions of the *GAL* promoter, the YNB medium was supplemented with a complete mixture Drop-out–uracil + 40 adenine (Formedium). Cells were grown overnight (till an OD_{640} of 1.2-1.8) in YNB medium with 2 % (w/v) glucose and then, after being washed twice in deionized water, they were transferred to YNB medium with 2 % (w/v) galactose at a starting OD_{640} of 0.2. Alternatively, cells were grown overnight (till an OD_{640} of 0.5) in YNB medium with 2 % (w/v) galactose (plus 0.1 %, w/v, glucose), as described by (Leung et al., 2010). Glucose (2 %, w/v) was added, when indicated.

Bioinformatic tools

The protein sequences were obtained in SGD (http://www.yeastgenome.org) and FungiDB (https://fungidb.org/fungidb/app) databases. The secondary structures were predicted by TOPCONS (Bernsel et al., 2009). Tertiary structures were predicted by HHpred (http://toolkit.tuebingen.mpg.de/hhpred) and MODELLER software (Šali et al., 1995), as described previously (Soares-Silva et al., 2007; Soares-Silva et al., 2011). The minimum number of residues predicted in this work for N- or C-terminus of Jen1 are listed in **Table S1**.

Alphafold predictions were accessed from the Alphafold Protein Structure Database (https://alphafold.ebi.ac.uk/) (Jumper et al., 2021; Varadi et al., 2022). Molecular graphics and analysis were performed with UCSF Chimera, developed by the Resource for Biocomputing, Visualization, and Informatics at the University of California, San Francisco, with support from NIH P41-GM103311 (Pettersen et al., 2004). Raytraced images were produced with POV-Ray x (http://www.povray.org/).

Construction of transporter truncations and chimeras

All constructions were performed by *in vivo* gap repair (Ma et al., 1987). Firstly, DNA fragments were amplified by PCR (Accuzyme DNA Polymerase, Bioline, or Supreme NZYProof DNA Polymerase, Nzytech) with specific oligonucleotides (listed in **Table S3**) using yeast genomic DNA (unless it is clearly specified). The resulting PCR products were co-transformed with a linearized plasmid (digested with a specific restriction enzyme) in *S. cerevisiae* cells. All plasmids used and constructed are listed in **Table S4**. Specifically, for construction of *JEN1* termini truncated versions pGPDJEN1ΔNT133, pGPDJEN1ΔCT33, pGPDJEN1ΔCT62, *JEN1* gene DNA fragments were amplified using the following oligonucleotides pairs, respectively: D-NTJEN1_133 and RCTJEN1; D-CTJEN1_33 and CYC1TERM; and D-CTJEN1_62 and CYC1TERM. The resulting PCR products were co-transformed with the linearized plasmid pGPDJEN1. For pGPDJEN1ΔNT94 and pGPDJEN1ΔNT94ΔCT33 constructions, the DNA fragments were amplified from pGPDJEN1 and pGPDJEN1ΔCT33, respectively, using the oligonucleotides Fw_GPD_jen1dNT94 and Rev_GFP_jen1. The resulting PCR products were co-transformed with the linearized plasmid p416GPD. For construction of *JEN1* termini truncated versions under the control of the *GAL* promoter: pGALJEN1ΔCT33, pGALJEN1ΔNT94 and pGPDJEN1ΔNT94ΔCT33, the *GAL* DNA fragment was amplified from pGALJEN1 with the oligonucleotides GPDfwd and GALrev for pGALJEN1ΔCT33 construction or with the oligonucleotides GPDfw_new and GALrev_dNT94 for constructions pGALJEN1ΔNT94 and pGPDJEN1ΔNT94ΔCT33. The resulting *GAL* PCR product were co-transformed with the respective linearized plasmid (pGPDJEN1ΔCT33, pGPDJEN1ΔNT94 or pGPDJEN1ΔNT94ΔCT33). For the construction of pGALUAPA/JEN1CT33, the *GALUAPA* DNA fragment was amplified from pDDGFP2UAPA using the primers 381 and UapA_rev_33; the *JEN1CT33* DNA fragment was amplified from pDDGFP2UAPAΔCT/JEN1CT62 using the primers Jen1_fw_ct33 and 317. These DNA fragments were then co-transformed with linearized p426GPD plasmid previously digested with *SacI* and *XhoI* restriction enzymes to remove the GPD promoter. The pDDGFP2UAPAΔCT/JEN1CT62 plasmid was derived from pDDGFP2UAPA (Leung et al., 2010). For the construction of pGALUAPA/JEN1NT94, the *GALJEN1NT94* DNA fragment was amplified from pGALJEN1 using the primers 381 and REV_Jen1_UapA; the *UAPAGFP* DNA fragment was amplified from pDDGFP2UAPA using the primers FW_UapA_Jen1

and 317. These DNA fragments were then co-transformed with linearized p426GPD plasmid previously digested with *SacI* and *XhoI* restriction enzymes to remove the GPD promoter. For the construction of pGALUAPA/JEN1NT94-CT33, *GALJEN1NT94* DNA fragment was amplified from pGALJEN1 using the primers 381 and REV_Jen1_UapA; the *UAPA/JEN1CT33GFP* DNA fragment was amplified from pGALUAPA/JEN1CT33 using the primers FW_UapA_Jen1 and 317. These DNA fragments were then co-transformed with linearized p426GPD plasmid previously digested with *SacI* and *XhoI* restriction enzymes to remove the GPD promoter. For the construction of pGALJEN1CT33/UAPA, *JEN1CT33* DNA fragment was amplified from pGPDJEN1 using the primers Fw-CT33-UapA and Rev-CT33-UapA. This DNA fragment was then co-transformed with linearized pGALUAPA/JEN1NT94 plasmid previously digested with *BamHI* restriction enzyme.

Plasmid isolation from *S. cerevisiae* and *E. coli* strains was performed by standard protocols. Transformations were performed by the standard lithium acetate/polyethylene glycol method (Gietz and Woods, 2002). All constructs were confirmed by DNA sequencing (GATC Biotech and MWG Eurofins).

Transport assays

Transport activity assays for Jen1 WT and Jen1 truncated transporters were performed as previously described (Soares-Silva et al., 2007) using radiolabelled D,L-[^{14}C] lactic acid (Amersham Biosciences). Yeast cells were mid-exponentially grown in glucose and transferred to a fresh 0.5 % (v/v) lactate medium for 4h (Lac 4h). For uptake measurements, yeast cells were harvested in Lac 4h and centrifuged (5000 rpm, 2 minutes). The samples were then washed twice with ice-cold deionized water and resuspended in ice-cold deionized water to a final concentration of about 20–40 mg dry weight/mL. The reaction mixtures were prepared in 1.5 mL tubes containing 60 µL of KH_2PO_4 (0.1 M, pH 5.0), and 30 µL of the yeast cell suspension. After incubation, the reaction was started by the addition of 10 µL of 6 mM radiolabelled lactic acid, pH 5.0 (specific activity 2000 dpm/nmol), rapidly mixed by vortexing, and incubated for 1 min. After one minute, 100 µL of 100 mM non-labelled substrate, was added, quickly mixed by vortexing and the mixture was chilled on ice, to stop the reaction. The reaction solutions were centrifuged for 5 min at 13200 rpm. The supernatant was rejected, and the pellet was resuspended in 1 mL of deionized

cold water and centrifuged for 5 min, at 13200 rpm. The resulting pellet was resuspended in 1 mL of scintillation liquid (Opti-Phase HiSafe II; LKB FSA Laboratory Supplies). Radioactivity was measured in a Packard TRI-CARB 4810 TR liquid scintillation spectrophotometer with disintegrations per minute correction. The % uptake rate of wild-type Jen1 (Jen1 WT) is considered 100 %. The data is represented as a scatter plot with bar (mean and SD) (Prism 9.0 (GraphPad software, version 9.2.0)) of all data points obtained in three independent experiments. For kinetic assays the methodology used was the same as described above for transport activity assays. However, in this case, the cells were exposed for 30 seconds to various concentrations of radiolabelled D, L-[^{14}C] lactic acid, ranging from 0.03 to 2 mM. The data is represented as a Michaelis-Menten plot of the net initial velocity relative to increasing lactic acid concentrations, showing the mean values of at least three independent experiments (n≥3). The error bars represent the standard deviation. K_m and V_{max} were determined using the Prism 9.0 (GraphPad software, version 9.2.0) with 95 % confidence interval and p values <0.0001. K_m, Michaelis-Menten constant; SE, standard error; V_{max}, maximum velocity. Transport activity assays for wild-type UapA and UapA-Jen1 chimeras were performed essentially as described in (Leung et al., 2010), using radiolabelled [^{3}H]-xanthine (21.1 Ci/mmol, Moravek Biochemicals, Brea, CA).

Phenotypic growth tests

Phenotypic growth assays on solid medium were performed according to (Soares-Silva et al., 2011; Talaia et al., 2017). A serial of 1:10 yeast cell dilutions (starting from an OD_{640} of 1) were performed and 3 µL of each yeast suspension were plated in YNB solid medium, containing the desired carbon source. Cells were incubated at 30 °C or 18 °C, for 4 or 7 days, respectively. Three independent experiments were performed.

Epifluorescence microscopy and quantifications

Yeast cells were grown, as described above, and visualized by fluorescent microscopy. A volume of 1 mL of growing yeast cells was collected and concentrated by a factor of 10. 5 µL of each sample was then directly visualized, without fixation, on a Leica DM5000B microscope with appropriate filters. For the vacuolar staining, cells were incubated for 10 min at 30 °C with 1.5 µL of CellTracker™ Blue CMAC (7-amino-4-chloromethylcoumarin) (Invitrogen). The resulting images were acquired with a Leica DFC 350FX R2 digital camera using the LAS AF software. Images were then processed in the Adobe Photoshop CC 2018 (Adobe Systems).

The quantification of the ratio between the fluorescence at the cell periphery and the total fluorescence, at the 4 h glucose treatment, was performed using ImageJ software (version 1.53k) as described in (Hovsepian et al., 2018). The data is represented as a scatter plot with median (n≥45 cells). An ordinary one-way ANOVA analysis was used followed by a Tukey´s multiple comparisons test using Prism 9.0 (GraphPad software, version 9.2.0). The p values are indicated (NS: $p > 0.05$; *, $p < 0.05$; **, $p < 0.01$; ***, $p < 0.001$; ****, $p < 0.0001$).

Measurement of yeast culture pH

The pH of the culture medium was determined as previously described (Talaia et al., 2017). A volume of 1 mL of cell culture was harvested and the pH value was immediately measured by a pHmeter (Braun). The data is represented as an interleaved scatter plot (mean and SD) (Prism 9.0 (GraphPad software, version 9.2.0)) of at least three independent experiments.

Western blot analysis and quantifications

Yeast cells were grown as above- mentioned and crude protein extracts were prepared as previously described (Paiva et al., 2009). Nitrocellulose membranes (GE Healthcare Life Sciences) were probed with the primary antibodies: anti-GFP (monoclonal anti-green fluorescent protein from mouse IgG1κ, clones 7.1 and 13.1, Roche, 11814460001) and anti-PGK (monoclonal anti-3-phosphoglycerate kinase from *S. cerevisiae*, clone 22C5D8, Invitrogen), used at 1:3000 and 1:10000 dilutions, respectively. The anti-mouse IgG (whole molecule)-peroxidase produced in rabbit

(A9044, Sigma) was used as a secondary antibody at 1:10000 dilution. The signal was detected by enhanced chemiluminescence using the WesternBright ECL HRP substrate (advansta). The membranes were exposed to X-ray films (Ortho CP-G Plus, Agfa) and the chemiluminescence signals were acquired using an automatic film processor (Curix 60, Afga).

The quantifications of the bands were performed using the ImageJ software (version 1.53k). The quantification levels of the Jen1-GFP signal were divided by the respective values of the PGK (used as a loading control). The relative levels of protein expression of the Jen1 truncations were normalized to Gal 5 h (set as 100 %). The data is represented as a column bar graph (mean with SEM) (Prism 9.0 (GraphPad software, version 9.2.0)) of at least three independent experiments.

For bimolecular fluorescence complementation (BiFC) assay

For BiFC analyses, several plasmid constructions were performed (**Table S4**): pGPDJEN1YFP$_N$ (URA3), pGPDJEN1YFP$_C$ (HIS3), pGPDYFP$_N$JEN1YFP$_C$ (URA3), pGPDYFP$_N$ (URA3) and pGPDYFP$_C$ (URA3), using a GAP repair cloning strategy. The N-terminal half of the yellow fluorescent protein (YFP$_N$; 154 AA residues of YFP), and the C-terminal half of YFP (YFP$_C$; 86 AA residues of YFP) were amplified from plasmids PDV7 and PDV8 (Zekert et al., 2010), respectively. *JEN1* ORF was amplified from pGPDJEN1 plasmid. The primers used are listed in **Table S3.**

To study the possible interaction of the Jen1 N- with C- terminus, *jen1*Δ cells expressing pGPDYFP$_N$JEN1YFP$_C$ were grown overnight in glycerol (3 %, v/v), supplemented with the required auxotrophies, until mid-exponential phase, to induce Jen1 expression at the PM. Then, a pulse of lactate (0.5 %, v/v) was added, and fluorescent images were acquired at the indicated time points. Cells co-expressing pGPDJEN1YFP$_N$ (URA3) and pGPDJEN1YFP$_C$ (HIS3) or expressing pGPDYFP$_N$ (URA3), pGPDYFP$_C$ (URA3) or pGPDJEN1GFP (URA3) were used as controls.

Acknowledgments

We thank Olivier Vincent and Bruno André for fruitful discussions. This work was supported by the “Contrato-Programa” UIDB/04050/2020 and by the project PTDC/BIA-MIC/5246/2020 funded by national funds through the “Fundação para a Ciência e a Tecnologia” (FCT) I.P. and by the European Regional Development

Fund (ERDF) through the COMPETE 2020 – “Programa Operacional Competitividade e Internacionalização” (POCI). GD was supported by "Fondation Sante" (KE17237). CBA and GT acknowledge FCT for the PD/BD/135208/2017 and SFRH/BD/86221/2012 PhD grants, respectively.

Conflict of Interest

The authors declare that they have no conflicts of interest with the contents of this article.

References

Alguel, Y., Amillis, S., Leung, J., Lambrinidis, G., Capaldi, S., Scull, N. J., Craven, G., Iwata, S., Armstrong, A., Mikros, E., et al. (2016). Structure of eukaryotic purine/H+ symporter UapA suggests a role for homodimerization in transport activity. *Nat. Commun.* **7**, 1–9.

Alvarez, C. E. (2008). On the origins of arrestin and rhodopsin. *BMC Evol. Biol.* **8**, 1–13.

Barata-Antunes, C., Alves, R., Talaia, G., Casal, M., Gerós, H., Mans, R. and Paiva, S. (2021). Endocytosis of nutrient transporters in fungi: The ART of connecting signaling and trafficking. *Comput. Struct. Biotechnol. J.* **19**, 1713–1737.

Becuwe, M. and Léon, S. (2014). Integrated control of transporter endocytosis and recycling by the arrestin-related protein Rod1 and the ubiquitin ligase Rsp5. *Elife* **3**, 1–23.

Becuwe, M., Herrador, A., Haguenauer-Tsapis, R., Vincent, O. and Léon, S. (2012a). Ubiquitin-mediated regulation of endocytosis by proteins of the arrestin family. *Biochem. Res. Int.* **2012**, 1–12.

Becuwe, M., Vieira, N., Lara, D., Gomes-Rezende, J., Soares-Cunha, C., Casal, M., Haguenauer-Tsapis, R., Vincent, O., Paiva, S. and Léon, S. (2012b). A molecular switch on an arrestin-like protein relays glucose signaling to transporter endocytosis. *J. Cell Biol.* **196**, 247–259.

Bernsel, A., Viklund, H., Hennerdal, A. and Elofsson, A. (2009). TOPCONS: Consensus prediction of membrane protein topology. *Nucleic Acids Res.* **37**, 465–468.

Bowton, E., Saunders, C., Reddy, I. A., Campbell, N. G., Hamilton, P. J., Henry, L. K., Coon, H., Sakrikar, D., Veenstra-VanderWeele, J. M., Blakely, R. D., et al. (2014). SLC6A3 coding variant Ala559Val found in two autism probands alters dopamine transporter function and trafficking. *Transl. Psychiatry* **4**, 1–11.

Crapeau, M., Merhi, A. and André, B. (2014). Stress conditions promote yeast Gap1 permease ubiquitylation and down-regulation via the arrestin-like bul and aly proteins. *J. Biol. Chem.* **289**, 22103–22116.

Diallinas, G. (2016). Dissection of Transporter Function: From Genetics to Structure. *Trends Genet.* **32**, 576–590.

Diallinas, G. and Martzoukou, O. (2019). Transporter membrane traffic and function: lessons from a mould. *FEBS J.* **286**, 4861–4875.

Fujita, S., Sato, D., Kasai, H., Ohashi, M., Tsukue, S., Takekoshi, Y., Gomi, K. and Shintani, T. (2018). The C-terminal region of the yeast monocarboxylate transporter Jen1 acts as a glucose signal-responding degron recognized by the α-arrestin Rod1. *J. Biol. Chem.* **293**, 10926–10936.

Ghaddar, K., Merhi, A., Saliba, E., Krammer, E.-M., Prevost, M. and Andre, B. (2014). Substrate-Induced Ubiquitylation and Endocytosis of Yeast Amino Acid Permeases. *Mol. Cell. Biol.* **34**, 4447–4463.

Gietz, R. D. and Woods, R. A. (2002). Transformation of yeast by lithium acetate/single-stranded carrier DNA/polyethylene glycol method. *Methods Enzymol.* **350**, 87–96.

Gonzalez-Menendez, P., Hevia, D., Mayo, J. C. and Sainz, R. M. (2017). The dark side of glucose transporters in prostate cancer: Are they a new feature to characterize carcinomas? *Int. J. cancer* **142**, 2414–2424.

Gournas, C., Amillis, S., Vlanti, A. and Diallinas, G. (2010). Transport-dependent endocytosis and turnover of a uric acid-xanthine permease. *Mol. Microbiol.* **75**, 246–60.

Gournas, C., Saliba, E., Krammer, E.-M., Barthelemy, C., Prévost, M. and André, B. (2017). Transition of yeast Can1 transporter to the inward-facing state unveils an α-arrestin target sequence promoting its ubiquitylation and endocytosis. *Mol. Biol. Cell* **28**, 2819–2832.

Guiney, E. L., Klecker, T. and Emr, S. D. (2016). Identification of the endocytic sorting signal recognized by the Art1-Rsp5 ubiquitin ligase complex. *Mol. Biol. Cell* **27**, 4043–4054.

Hovsepian, J., Albanèse, V., Becuwe, M., Ivashov, V., Teis, D. and Léon, S. (2018). The yeast arrestin-related protein Bul1 is a novel actor of glucose-induced endocytosis. *Mol. Biol. Cell* **33**, 1012–1020.

Jumper, J., Evans, R., Pritzel, A., Green, T., Figurnov, M., Ronneberger, O., Tunyasuvunakool, K., Bates, R., Žídek, A., Potapenko, A., et al. (2021). Highly accurate protein structure prediction with AlphaFold. *Nature* **596**, 583–589.

Kahlhofer, J., Leon, S., Teis, D. and Schmidt, O. (2020). The α-arrestin family of ubiquitin ligase adaptors links metabolism with selective endocytosis. *Biol. Cell* **113**, 1–59.

Karachaliou, M., Amillis, S., Evangelinos, M., Kokotos, A. C., Yalelis, V. and Diallinas, G. (2013). The arrestin-like protein ArtA is essential for ubiquitination and endocytosis of the UapA transporter in response to both broad-range and specific signals. *Mol. Microbiol.* **88**, 301–317.

Keener, J. M. and Babst, M. (2013). Quality Control and Substrate-Dependent Downregulation of the Nutrient Transporter Fur4. *Traffic* **14**, 412–427.

Kim, H., Lee, W. H., Galazka, J. M., Cate, J. H. D. and Jin, Y. S. (2014). Analysis of cellodextrin transporters from Neurospora crassa in Saccharomyces cerevisiae for cellobiose fermentation. *Appl. Microbiol. Biotechnol.* **98**, 1087–1094.

Knychala, M. M., dos Santos, A. A., Kretzer, L. G., Gelsleichter, F., Leandro, M. J., Fonseca, C. and Stambuk, B. U. (2022). Strategies for Efficient Expression of Heterologous Monosaccharide Transporters in Saccharomyces cerevisiae. *J. Fungi* **8**, 84.

Leung, J., Karachaliou, M., Alves, C., Diallinas, G. and Byrne, B. (2010). Expression and purification of a functional uric acid-xanthine transporter (UapA). *Protein Expr. Purif.* **72**, 139–46.

Lin, C. H., MacGurn, J. A., Chu, T., Stefan, C. J. and Emr, S. D. (2008). Arrestin-Related Ubiquitin-Ligase Adaptors Regulate Endocytosis and Protein Turnover at the Cell Surface. *Cell* **135**, 714–725.

Ma, H., Kunes, S., Schatz, P. J. and Botstein, D. (1987). Plasmid construction by homologous recombination in yeast. *Gene* **58**, 201–16.

Manford, A. G., Stefan, C. J., Yuan, H. L., MacGurn, J. A. and Emr, S. D. (2012). ER-to-Plasma Membrane Tethering Proteins Regulate Cell Signaling and ER Morphology. *Dev. Cell* **23**, 1129–1140.

Marchal, C., Haguenauer-Tsapis, R. and Urban-Grimal, D. (1998). A PEST-like sequence mediates phosphorylation and efficient ubiquitination of yeast uracil permease. *Mol. Cell. Biol.* **18**, 314–21.

Marchal, C., Haguenauer-Tsapis, R. and Urban-Grimal, D. (2000). Casein kinase I-dependent phosphorylation within a PEST sequence and ubiquitination at nearby lysines signal endocytosis of yeast uracil permease. *J. Biol. Chem.* **275**, 23608–14.

Merhi, A. and Andre, B. (2012). Internal Amino Acids Promote Gap1 Permease Ubiquitylation via TORC1/Npr1/14-3-3-Dependent Control of the Bul Arrestin-Like Adaptors. *Mol. Cell. Biol.* **32**, 4510–4522.

Merhi, A., Gérard, N., Lauwers, E., Prévost, M. and André, B. (2011). Systematic mutational analysis of the intracellular regions of yeast Gap1 permease. *PLoS One* **6**, 1–12.

Mikros, E. and Diallinas, G. (2019). Tales of tails in transporters. *Open Biol.* **9**, 1–17.

Morgan, B. J., Chai, S. Y. and Albiston, A. L. (2011). GLUT4 associated proteins as therapeutic targets for diabetes. *Recent Pat. Endocr. Metab. Immune Drug Discov.* **5**, 25–32.

Nikko, E. and Pelham, H. R. B. (2009). Arrestin-mediated endocytosis of yeast plasma membrane transporters. *Traffic* **10**, 1856–1867.

Novoselova, T. V., Zahira, K., Rose, R. S. and Sullivan, J. A. (2012). Bul proteins, a nonredundant, antagonistic family of ubiquitin ligase regulatory proteins. *Eukaryot. Cell* **11**, 463–470.

O'Donnell, A. F., Apffel, A., Gardner, R. G. and Cyert, M. S. (2010). α-Arrestins Aly1 and Aly2 Regulate Intracellular Trafficking in Response to Nutrient Signaling. *Mol. Biol. Cell* **21**, 3552–3566.

Paiva, S., Vieira, N., Nondier, I., Haguenauer-Tsapis, R., Casal, M. and Urban-Grimal, D. (2009). Glucose-induced ubiquitylation and endocytosis of the yeast Jen1 transporter: role of lysine 63-linked ubiquitin chains. *J. Biol. Chem.* **284**, 19228–36.

Papadaki, G. F., Amillis, S. and Diallinas, G. (2017). Substrate specificity of the furE transporter is determined by cytoplasmic terminal domain interactions. *Genetics* **207**, 1387–1400.

Papadaki, G. F., Lambrinidis, G., Zamanos, A., Mikros, E. and Diallinas, G. (2019). Cytosolic N- and C-Termini of the Aspergillus nidulans FurE Transporter Contain Distinct Elements that Regulate by Long-Range Effects Function and Specificity. *J. Mol. Biol.* **431**, 3827–3844.

Pettersen, E. F., Goddard, T. D., Huang, C. C., Couch, G. S., Greenblatt, D. M., Meng, E. C. and Ferrin, T. E. (2004). UCSF Chimera - A visualization system for exploratory research and analysis. *J. Comput. Chem.* **25**, 1605–1612.

Rauch, S. and Martin-Serrano, J. (2011). Multiple interactions between the ESCRT machinery and arrestin-related proteins: implications for PPXY-dependent budding. *J. Virol.* **85**, 3546–3556.

Sakrikar, D., Mazei-Robison, M. S., Mergy, M. A., Richtand, N. W., Han, Q., Hamilton, P. J., Bowton, E., Galli, A., Veenstra-VanderWeele, J., Gill, M., et al. (2012). Attention Deficit/Hyperactivity Disorder-Derived Coding Variation in the Dopamine Transporter Disrupts Microdomain Targeting and Trafficking Regulation. *J. Neurosci.* **32**, 5385–5397.

Šali, A., Potterton, L., Yuan, F., van Vlijmen, H. and Karplus, M. (1995). Evaluation of comparative protein modeling by MODELLER. *Proteins Struct. Funct. Genet.* **23**, 318–326.

Scheffner, M. and Kumar, S. (2014). Mammalian HECT ubiquitin-protein ligases: Biological and pathophysiological aspects. *Biochim. Biophys. Acta - Mol. Cell Res.* **1843**, 61–74.

Soares-Silva, I., Schuller, D., Andrade, R. P., Baltazar, F., Cássio, F. and Casal, M. (2003). Functional expression of the lactate permease Jen1p of Saccharomyces cerevisiae in Pichia pastoris. *Biochem. J.* **376**, 781–787.

Soares-Silva, I., Paiva, S., Diallinas, G. and Casal, M. (2007). The conserved sequence NXX[S/T]HX[S/T]QDXXXT of the lactate/pyruvate:H(+) symporter subfamily defines the function of the substrate translocation pathway. *Mol. Membr. Biol.* **24**, 464–74.

Soares-Silva, I., Sá-Pessoa, J., Myrianthopoulos, V., Mikros, E., Casal, M. and Diallinas, G. (2011). A substrate translocation trajectory in a cytoplasm-facing topological model of the monocarboxylate/H(+) symporter Jen1p. *Mol. Microbiol.* **81**, 805–17.

Talaia, G., Gournas, C., Saliba, E., Barata-Antunes, C., Casal, M., André, B., Diallinas, G. and Paiva, S. (2017). The α-Arrestin Bul1p Mediates Lactate Transporter Endocytosis in Response to Alkalinization and Distinct Physiological Signals. *J. Mol. Biol.* **429**, 3678–3695.

Tanaka, M., Hiramoto, T., Tada, H., Shintani, T. and Gomi, K. (2017). Improved α-Amylase Production by Dephosphorylation Mutation of CreD, an Arrestin-Like Protein Required for Glucose-Induced Endocytosis of Maltose Permease and Carbon Catabolite Derepression in Aspergillus oryzae. *Appl Env. Microbiol.* **83**, 1–15.

Varadi, M., Anyango, S., Deshpande, M., Nair, S., Natassia, C., Yordanova, G., Yuan, D., Stroe, O., Wood, G., Laydon, A., et al. (2022). AlphaFold Protein Structure Database: massively expanding the structural coverage of protein-sequence space with high-accuracy models. *Nucleic Acids Res.* **50**, D439–D444.

Yashiroda, H., Oguchi, T., Yasuda, Y., Toh-E, A. and Kikuchi, Y. (1996). Bul1, a new protein that binds to the Rsp5 ubiquitin ligase in Saccharomyces cerevisiae. *Mol. Cell. Biol.* **16**, 3255–3263.

Zekert, N., Veith, D. and Fischer, R. (2010). Interaction of the Aspergillus nidulans microtubule-organizing center (MTOC) component ApsB with gamma-tubulin and evidence for a role of a subclass of peroxisomes in the formation of septal MTOCs. *Eukaryot. Cell* **9**, 795–805.

Figures

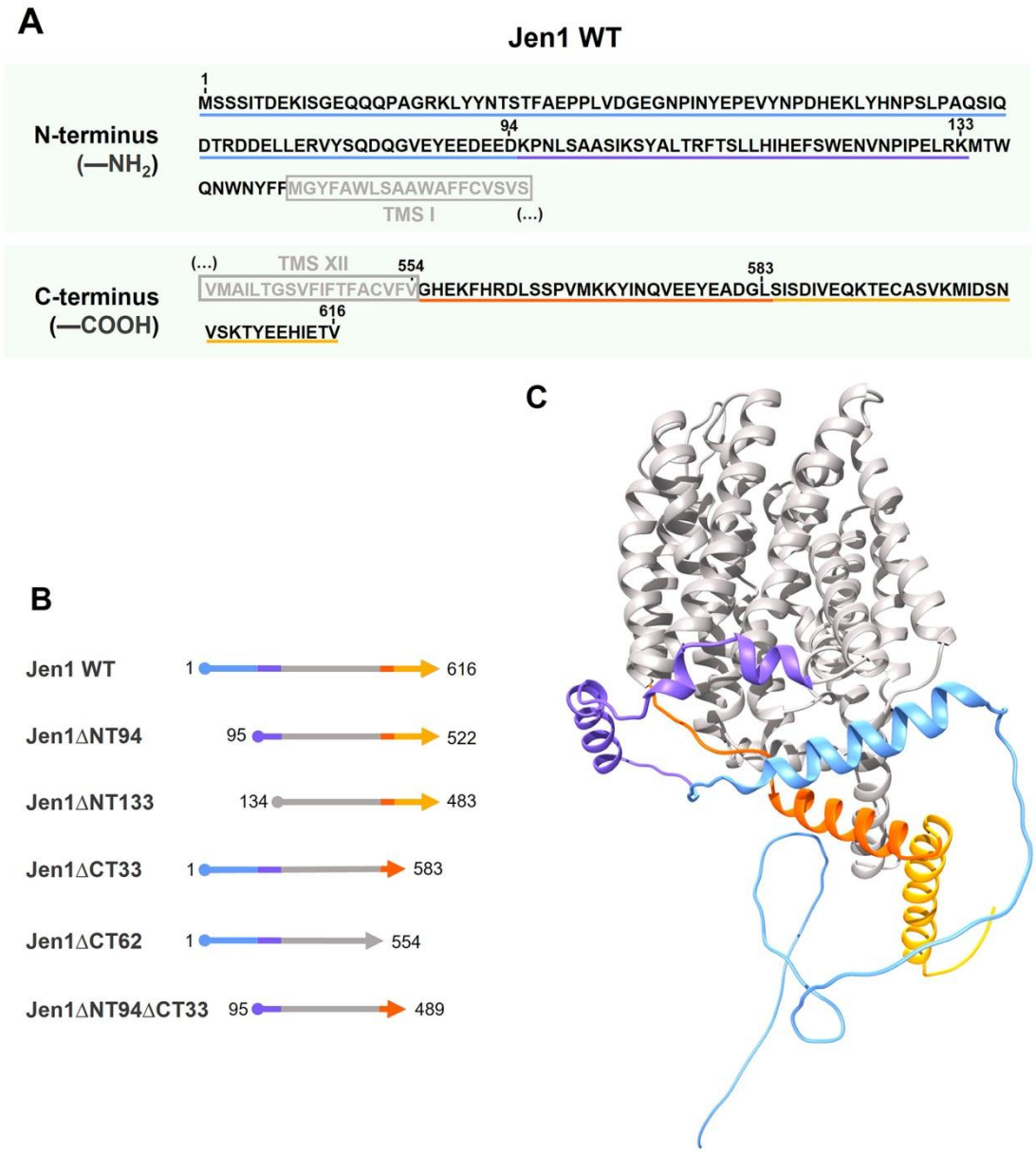

Figure 1 - **Designing of truncated versions of Jen1. (A) Primary amino acid sequences of the N- and C-terminal regions of Jen1 transporter**. N- and C-terminal predicted regions of Jen1 transporter are shown in black letters. The number of residues corresponding to these regions is indicated. Residues framed in grey correspond to predicted first or last transmembrane segments (TMSI and TMSXII, respectively), as defined by secondary prediction programs (see in

Experimental Procedures). (**B**) **Graphical representation of truncated Jen1 versions**. The Jen1 core protein is showed in light grey, the N- terminus region between amino acids 1-94 is in light blue, the region between 94-133 is in dark blue. Dark orange represents the predicted C-terminal region from 555 to 583 amino acids, while light orange represents the region of amino acid residues from 584 to 616. These regions are also underlined in panel A. Jen1 mutant versions were cloned either under the control of the strong *GPD* (glyceraldehyde-3-phosphate dehydrogenase) promoter, which allows the constitutive expression of *JEN1* (Soares-Silva et al., 2003), or under the control of the *GAL* promoter, enabling the expression of *JEN1*, under galactose (2 %, w/v) inducible conditions. (**C**) **Jen1 structure as predicted by Alphafold**. The predicted topology of the short and long truncations on both N- and C-termini is highlighted. The colour codes represent the same regions described above.

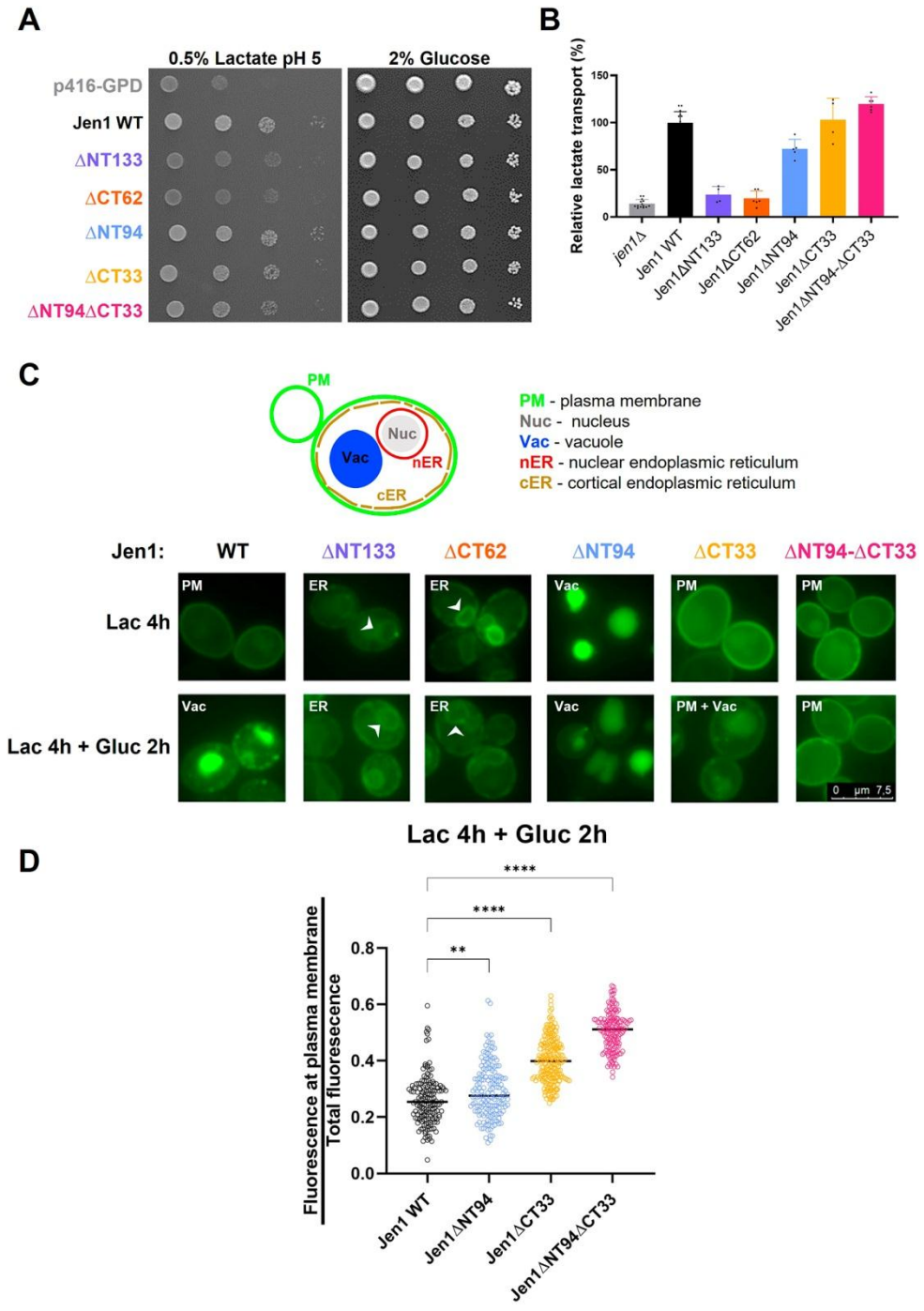

Figure 2 - Removing specific segments of Jen1 cytoplasmic N- and C- termini alters localization and transport activity. *S. cerevisiae jen1*Δ cells carrying the empty p416-GPD plasmid (*jen1*Δ) or either expressing full-length Jen1 (Jen1 WT) or the truncated Jen1 proteins (Jen1ΔCT33, Jen1ΔCT62, Jen1ΔNT133, Jen1ΔNT94, or Jen1ΔNT94ΔCT33), tagged with GFP, were characterized by growth assays (**A**), ^{14}C-lactic acid transport (**B**) and epifluorescence microscopy (**C**). (**A**) Serial 1:10

dilutions of yeast cells were spotted onto YNB containing plates supplemented with distinct carbon sources: glucose (2 %, w/v) or lactate (0.5 %, v/v, pH 5.0). Cells were grown for 7 days at 18 ^{0} C. (**B**) Percentage of ^{14}C-lactic acid uptake, at pH 5.0, in YNB lactic acid-derepressed cells. The rate of wild-type Jen1 is taken as 100 %. The mean of individual data points of at least three independent experiments (n≥3) are shown. Error bars correspond to standard deviation values. (**C**) **Top panel:** schematic representation of a yeast cell showing the main localizations of Jen1 or Jen1 truncated versions analysed in this study. **Bottom panels:** Epifluorescence microscopy analysis of Jen1-GFP or its derivatives. Cells were grown to mid-log in glucose, and samples were collected after growth in lactate medium for 4 hours (Lac 4 h) and after 2 hours of a pulse of glucose (Lac 4 h + Gluc 2 h). White arrows point to GFP fluorescence signal internal rings, typical of nuclear ER in yeast. The primary localization of the Jen1 constructs is described at the top left corner of each fluorescence microscopy image. PM, plasma membrane; ER, endoplasmic reticulum; Vac, vacuole. (**D**) At the time point Lac 4 h + Gluc 2 h, quantifications of the ratio of the fluorescence at the plasma membrane over the total fluorescence were made using the ImageJ software (version 1.53k) (see material and methods). The data is represented as a scatter plot with median (n≥150 cells). An ordinary one-way ANOVA analysis was used followed by a Tukey´s multiple comparisons test using Prism 9.0 (GraphPad software, version 9.2.0). The p values are indicated (NS: $p > 0.05$; *, $p < 0.05$; **, $p < 0.01$; ***, $p < 0.001$; ****, $p < 0.0001$).

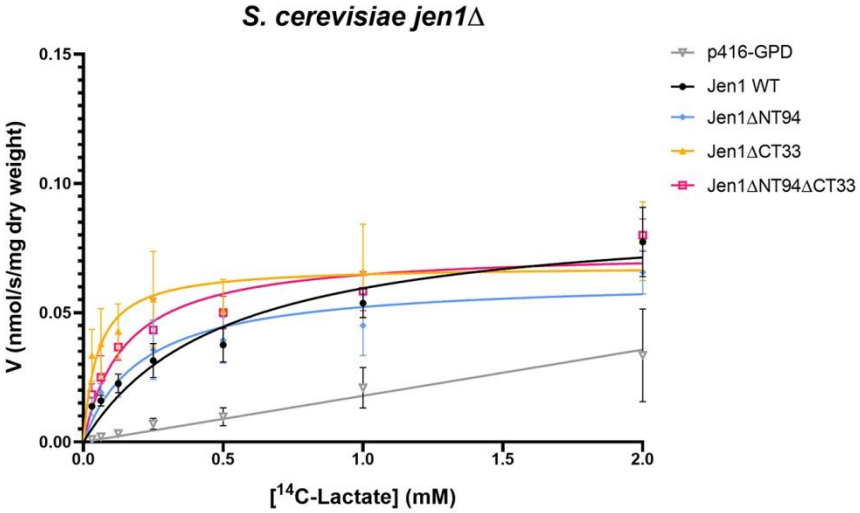

	Lactate	
	Kinetic parameters (± SE)	
Transporter	K_m (mM)	V_{max} (nmol/s/mg dry weight)
Jen1 WT	0.501 ± 0.097	0.089 ± 0.007
Jen1ΔNT94	0.210 ± 0.046	0.063 ± 0.004
Jen1ΔCT33	0.050 ± 0.015	0.068 ± 0.004
Jen1ΔNT94ΔCT33	0.148 ± 0.026	0.074 ± 0.004

Figure 3 - Transport kinetics of Jen1 truncations. The upper panel shows initial uptake rates of radiolabelled ^{14}C-lactic acid, pH 5.0, as a function of lactate concentration in *S. cerevisiae jen1*Δ cells expressing *JEN1* gene (Jen1 WT), *JEN1* mutant versions (Jen1ΔNT94, Jen1ΔCT33 and Jen1ΔNT94ΔCT33), or transformed with p416-GPD (empty vector) as a control. The respective kinetic parameters are highlighted in the table (lower panel). The data shown are mean values of at least three independent experiments (n≥3) and the error bars represent the standard deviation. K_m and V_{max} were determined using the GraphPad Prism 9.0 with 95 % confidence interval and p values <0.0001. K_m, Michaelis-Menten constant; SE, standard error; V_{max}, maximum velocity.

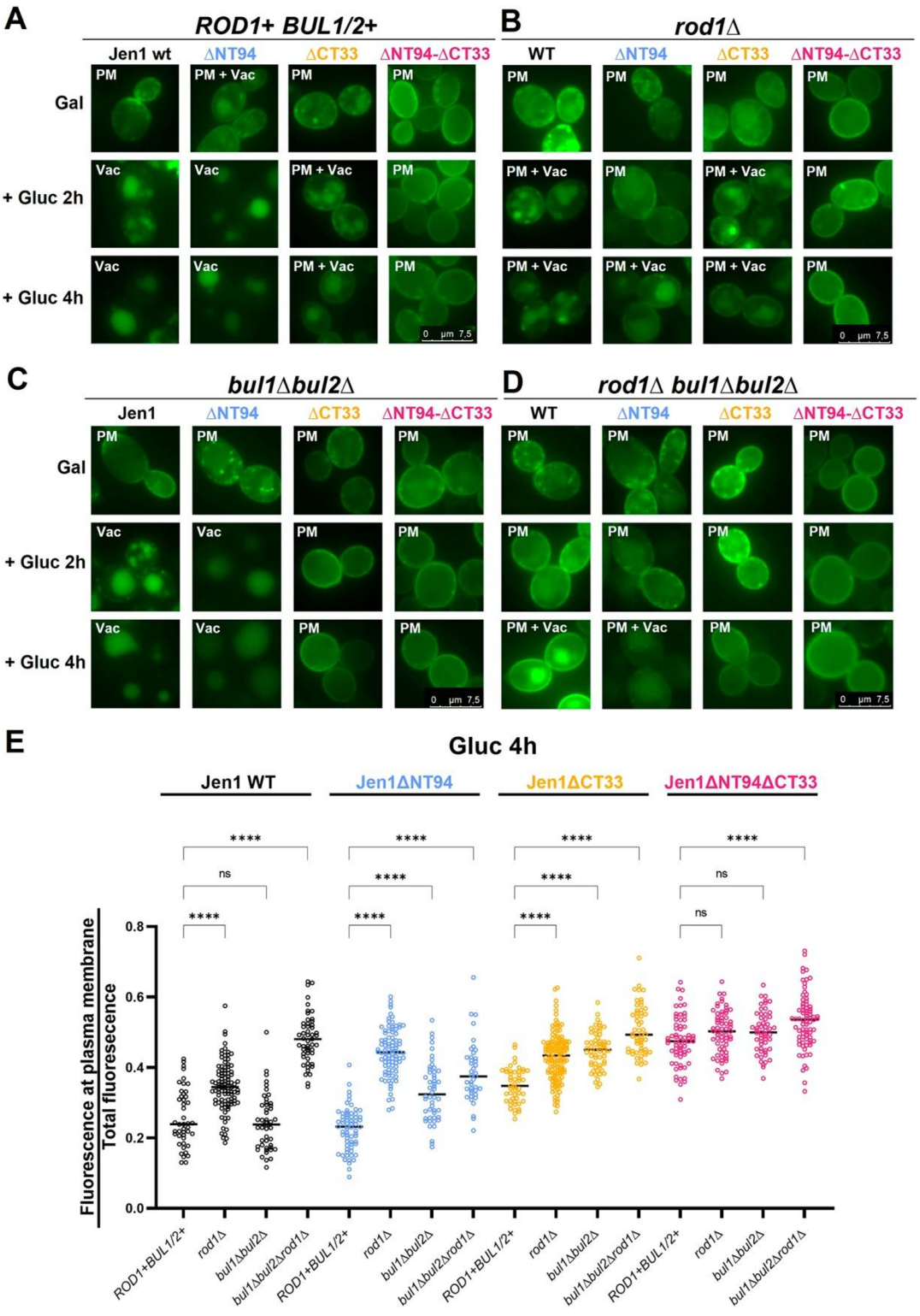

Figure 4 - Jen1 N- and C- termini are both involved in glucose-induced downregulation. Cells of *S. cerevisiae ROD1+ BUL1/2+*, *rod1*Δ, *bul1*Δ*bul2*Δ or *rod1*Δ*bul1*Δ*bul2*Δ, expressing the Jen1 truncations tagged with *GFP* and expressed under a *GAL* promoter were analysed by epifluorescence microscopy. The primary localization of the Jen1 constructs is described at the top left corner of each

fluorescence image panel. PM, plasma membrane; ER, endoplasmic reticulum; Vac, vacuole (**A**-**D**). Cells expressing Jen1 WT and Jen1 truncations (Jen1ΔNT94, Jen1ΔCT33 or Jen1ΔNT94ΔCT33) were grown overnight in YNB glucose (2 %, w/v) medium and, after being washed twice in deionized water, cells were transferred to YNB galactose (2 %, w/v) medium to induce Jen1 expression of the Jen1 constructs. After 5 h in galactose medium, glucose was added. Cells were visualized by fluorescent microscopy at specific time points (Gal 5 h, Gal 5 h + Gluc 2 h and Gal 5 h + Gluc 4 h). At the time point Gluc 4 h, quantifications of the ratio of the fluorescence at the plasma membrane over the total fluorescence were made using the ImageJ software (version 1.53k) (see material and methods. The data is represented as a scatter plot with median (n≥45 cells). An ordinary one-way ANOVA analysis was used followed by a Tukey´s multiple comparisons test using Prism 9.0 (GraphPad software, version 9.2.0). The p values are indicated (NS: $p > 0.05$; *, $p < 0.05$; **, $p < 0.01$; ***, $p < 0.001$; ****, $p < 0.0001$) **(E)**.

A

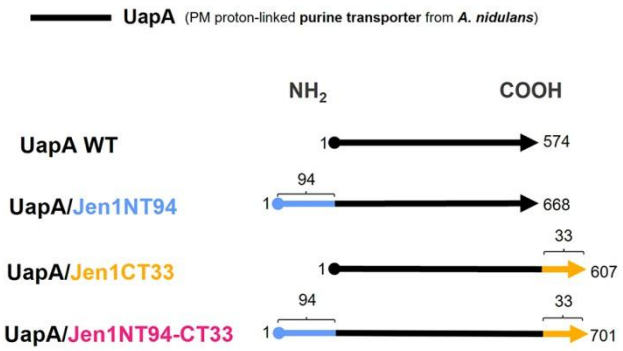

B

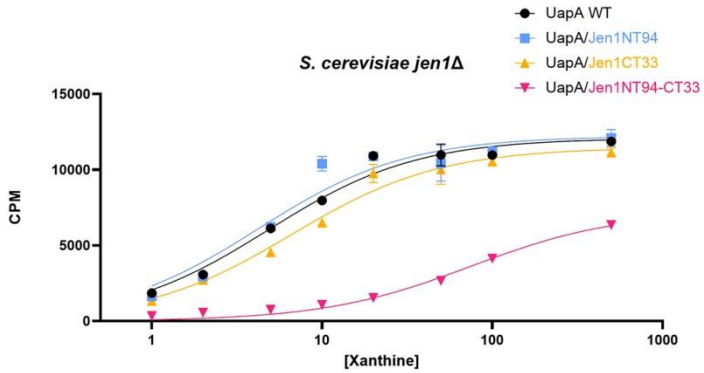

	Xanthine	
	Kinetic parameters (± SE)	
Transporter	K_m (μM)	V_{max} (%)
UapA WT	4.866 ± 1.365	100.00 ± 0.064
UapA/Jen1NT94	4.244 ± 2.028	101.12 ± 0.106
UapA/Jen1CT33	6.668 ± 2.163	94.88 ± 0.073
UapA/Jen1NT94-CT33	74.76 ± 24.646	59.93 ± 0.070

Figure 5 - Graphical representation (A) and transport kinetics (B) of the Jen1-UapA chimeric proteins. (**A**) The purine transporter UapA from *A. nidulans* is represented in black, the N- terminal region (1-94 amino acids) of the *S. cerevisiae* lactate transporter Jen1 is represented in light blue, while the C-terminal segment (the region of amino acid residues from 584 to 616) is colored in light orange. UapA-Jen1 chimeras were cloned under the control of the *GAL* promoter, enabling the expression of chimeras, under galactose (2 %, w/v) inducible conditions. (**B**) Cells of *S. cerevisiae ROD1+ BUL1/2+* strain expressing UapA-Jen1 chimeras tagged with

GFP were analysed by transport assays using radiolabelled xanthine (see Materials and methods and (Leung et al., 2010)). The respective kinetic parameters are highlighted in the table (lower panel). The data shown are mean values of at least three independent experiments (n≥3) and the error bars represent the standard deviation. K_m and V_{max} were determined using the GraphPad Prism 9.0 with 95 % confidence interval and p values <0.0001. K_m, Michaelis-Menten constant; SE, standard error; V_{max}, maximum velocity.

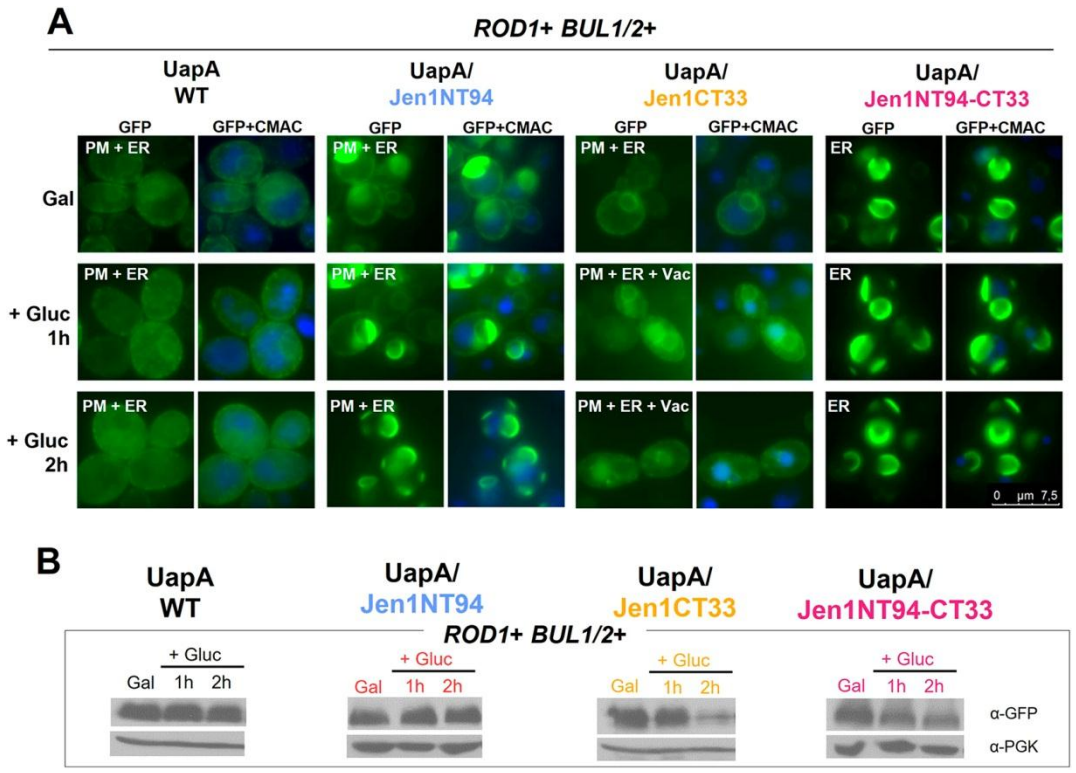

Figure 6 - The CT33 segment of Jen1 fused at the UapA C-terminus confers sensitivity to glucose-triggered endocytosis to UapA. Cells of *S. cerevisiae ROD1+ BUL1/2+* strain**,** expressing UapA-Jen1 chimeras tagged with *GFP* and expressed under a *GAL* promoter, were analysed by epifluorescence microscopy (**A**) and by Western blot (**B**). Cells were grown overnight in YNB galactose (2 %, w/v) + glucose (0.1 %, w/v) medium until mid-exponential phase and glucose was added when indicated (Gal + Gluc 1 h and Gal + Gluc 2 h). At these time points, cells were visualized by Fluorescent Microscopy and protein extracts were prepared for western immunoblotting with an anti-GFP antibody or anti-phosphoglycerate kinase (PGK) antibody (loading control). The blue CMAC dye was used as a vacuolar staining marker. The primary localization of the Jen1 constructs is described at the top left corner of each fluorescence image panel. All experiments were repeated at least 3 times (n≥3). PM, plasma membrane; ER, endoplasmic reticulum; Vac, vacuole.

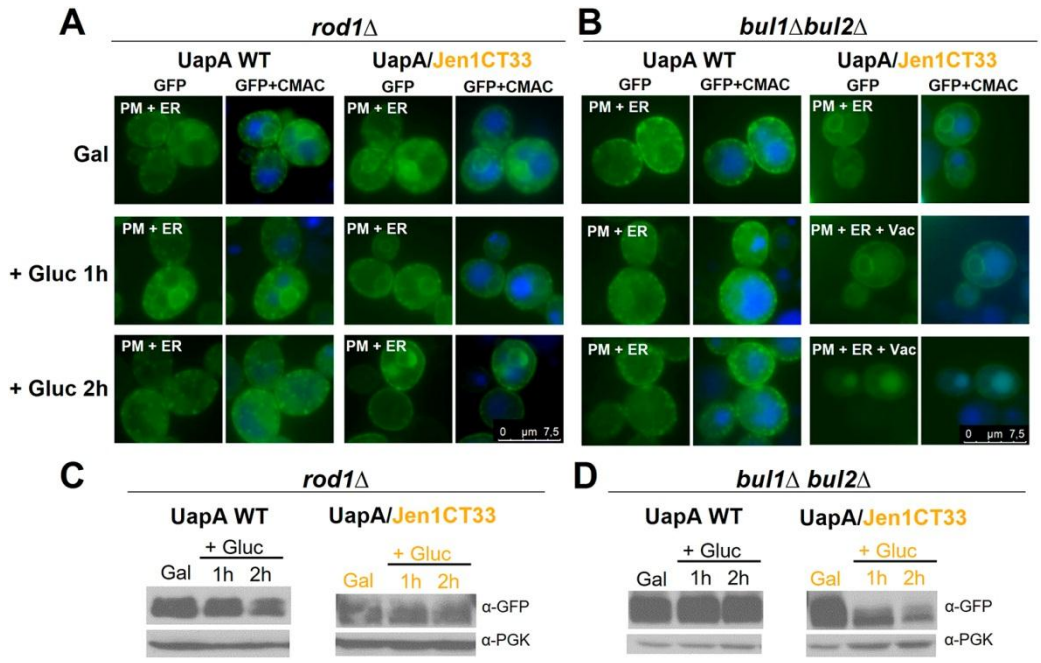

Figure 7 - Rod1 arrestin is involved in glucose-induced downregulation of UapA/Jen1CT33. Cells of *S. cerevisiae* lacking the arrestins *rod1*Δ or *bul1*Δ*bul2*Δ, expressing UapA or UapA/Jen1CT33 chimera tagged with *GFP* and expressed under a *GAL* promoter, were analysed epifluorescence microscopy (**A-B**) and by Western blot (**C-D**). Cells were grown overnight in YNB galactose (2 %, w/v) + glucose (0.1 %, w/v) medium until mid-exponential phase and glucose was added when indicated (Gal + Gluc 1 h and Gal + Gluc 2 h). At these time points, cells were visualized by Fluorescent Microscopy and protein extracts were prepared for western immunoblotting with an anti-GFP antibody or anti-phosphoglycerate kinase (PGK) antibody (loading control). The blue CMAC dye was used as a vacuolar staining marker. All experiments were repeated at least 3 times (n≥3).

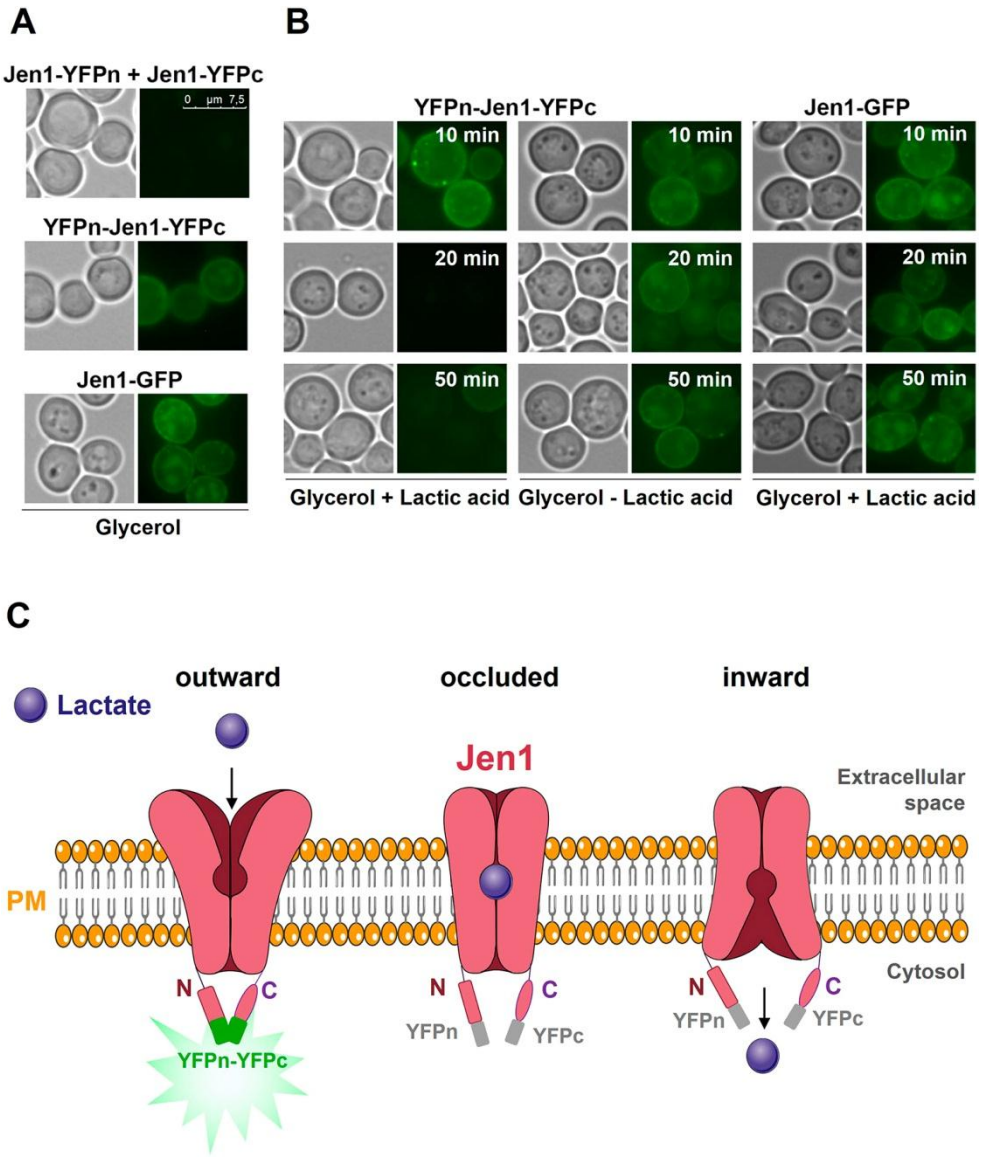

Figure 8 - The cytosolic termini of Jen1 come into close proximity in the absence of its substrate. Cells of *S. cerevisiae jen1*Δ strain expressing YFPn-Jen1-YFPc, or co-expressing both Jen1-YFPn and Jen1-YFPc were analysed by *in vivo* epifluorescence microscopy (for more details see Materials and Methods). (**A**) To induce Jen1 expression at the plasma membrane (PM), cells were grown in YNB 3 % (v/v) glycerol, until mid-exponential phase. (**B**) 0.5 % (v/v) lactic acid was added to cells previously grown in YNB 3 % (v/v) glycerol, until mid-exponential phase, and samples were collected over time for fluorescent microscopy analysis (left panel). As a negative control, the same experiment was performed without adding lactic acid (middle panel). Additionally, cells expressing *JEN1-GFP* were also tested, in the

presence of lactic acid for the same time points, in order to exclude the possibility of substrate-induced downregulation of Jen1 (right panel). All experiments were repeated at least 3 times (n≥3). (**C**) Speculative model of the Jen1 transporter termini conformation during a substrate transport cycle (i.e., outward-facing, occluded, inward-facing). In the absence of substrate, Jen1 is in an outward-facing conformation with the N- and C- termini in close contact or interacting with each other. Upon substrate addition, Jen1 moves to an inward conformation with consequent loss of termini interaction/proximity. The topological changes in Jen1 termini are crucial for Jen1 endocytic turnover, biogenesis/folding, transport activity and trafficking.

Table S1. Number of residues comprising the N- and C-termini of the Jen1 transporter predicted by structure-based programs.

Transporter	Domain	Number of amino acids	Prediction
Jen1	N-terminal	133	2^{ary} structure
	C-terminal	62	2^{ary} structure
		33	3^{ary} structure

The secondary structure was predicted by TOPCONS (Bernsel et al., 2009), while the tertiary structure was template-based modelled by HHpred using YajR (Zimmermann et al., 2018).

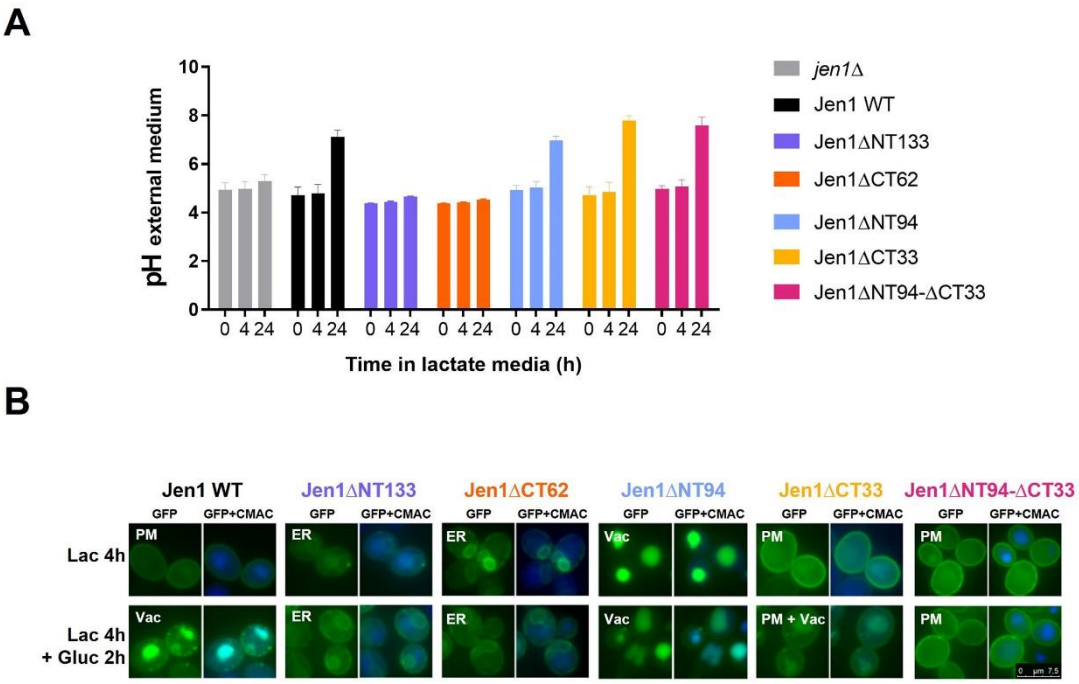

Fig. S1.Removing specific segments of Jen1 cytoplasmic N- and C- termini modifies transport kinetics and protein PM localization. *S. cerevisiae jen1*Δ cells expressing the empty p416-GPD plasmid vector (*jen1*Δ), the *JEN1* gene (Jen1 WT), or five *JEN1* truncated versions (Jen1ΔNT133, Jen1ΔCT62, Jen1ΔNT94, Jen1ΔCT33 and Jen1ΔNT94ΔCT33), tagged with *GFP*, were characterized by their effect on the pH of the culture medium (**A**) and by epifluorescence microscopy (**B**).
(**A**) The pH of the culture medium was measured, during lactate growth, at the indicated time points (0 h, 4 h, and 24 h). The mean of individual data points of at least three independent experiments (n≥3) are shown and error bars represent standard deviation.
(**B**) Epifluorescence microscopy analysis of Jen1-GFP or its derivatives. Samples were collected after growth in lactate medium for 4 hours (Lac 4 h) and after 2 hours of addition of glucose (2 %, w/v) to 4 h Lac-induced cells (Lac 4 h + Gluc 2 h) The blue CMAC dye was used as a vacuolar staining marker.

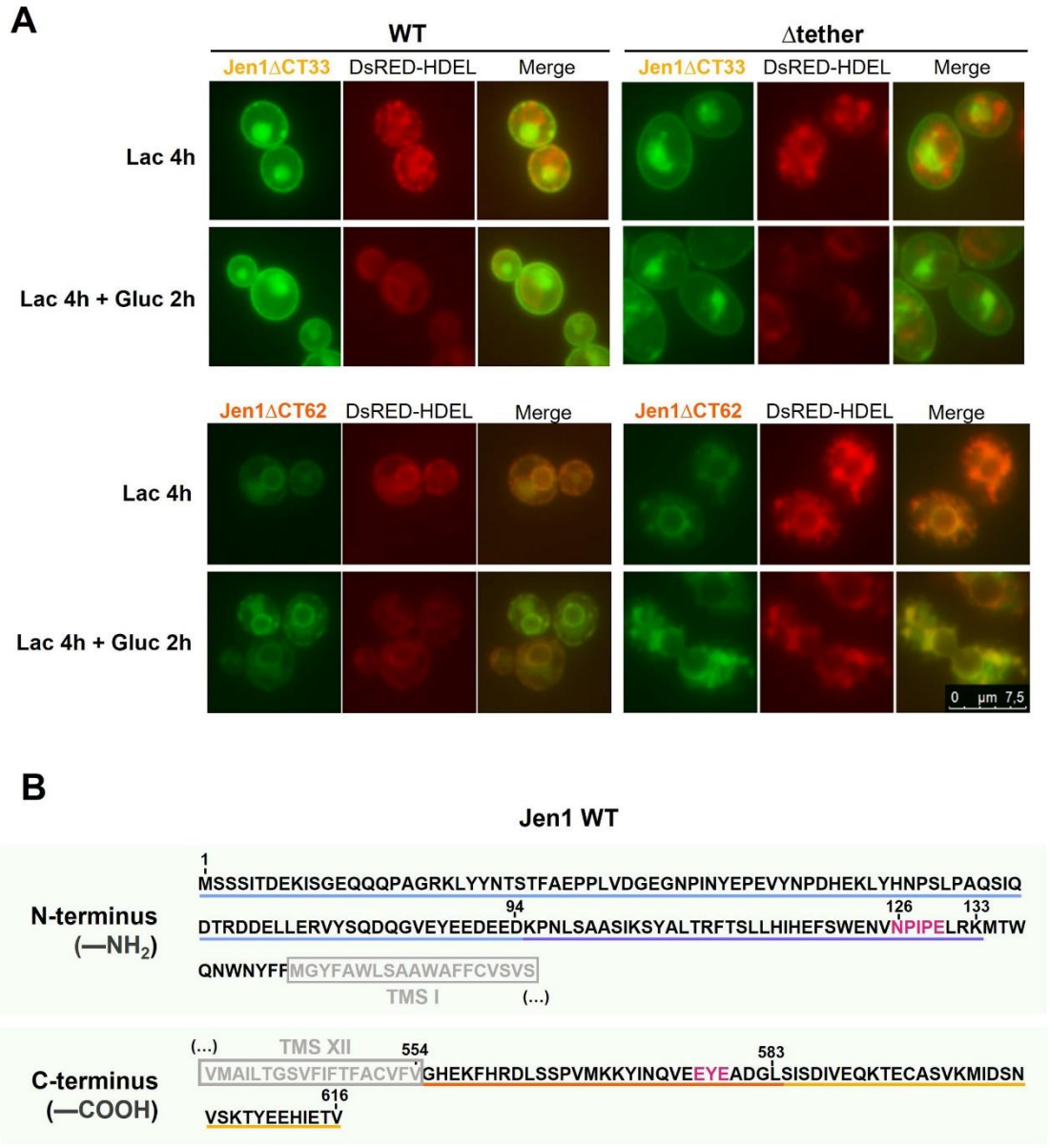

Fig. S2. **The cytosolic termini of Jen1 are essential for ER-exit and proper sorting to the PM. (A)** Epifluorescence microscopy examination of wild type control cells (WT) or Δtether cells expressing the ER marker DsRed-HDEL (Manford et al., 2012) and Jen1ΔCT62-GFP. Cells were grown in YNB glucose (2 %, w/v) medium until mid-exponential phase. They were then washed in deionized water and transferred to fresh YNB lactate (0.5 %, v/v) medium (Lac 4 h) to induce Jen1 expression. After 4 h, glucose was added (Lac 4 h + Gluc 2 h). Note that JenΔCT62 co-localizes with the ER marker DsRed-HDEL in both WT and Δtether cells demonstrating ER retention of this mutant protein. (**B**) The amino acid sequences of the N- and C- termini of Jen1 contain potential ER exit motifs (^{126}NPIPE^{133} and ^{577}EYE^{579} highlighted in pink).

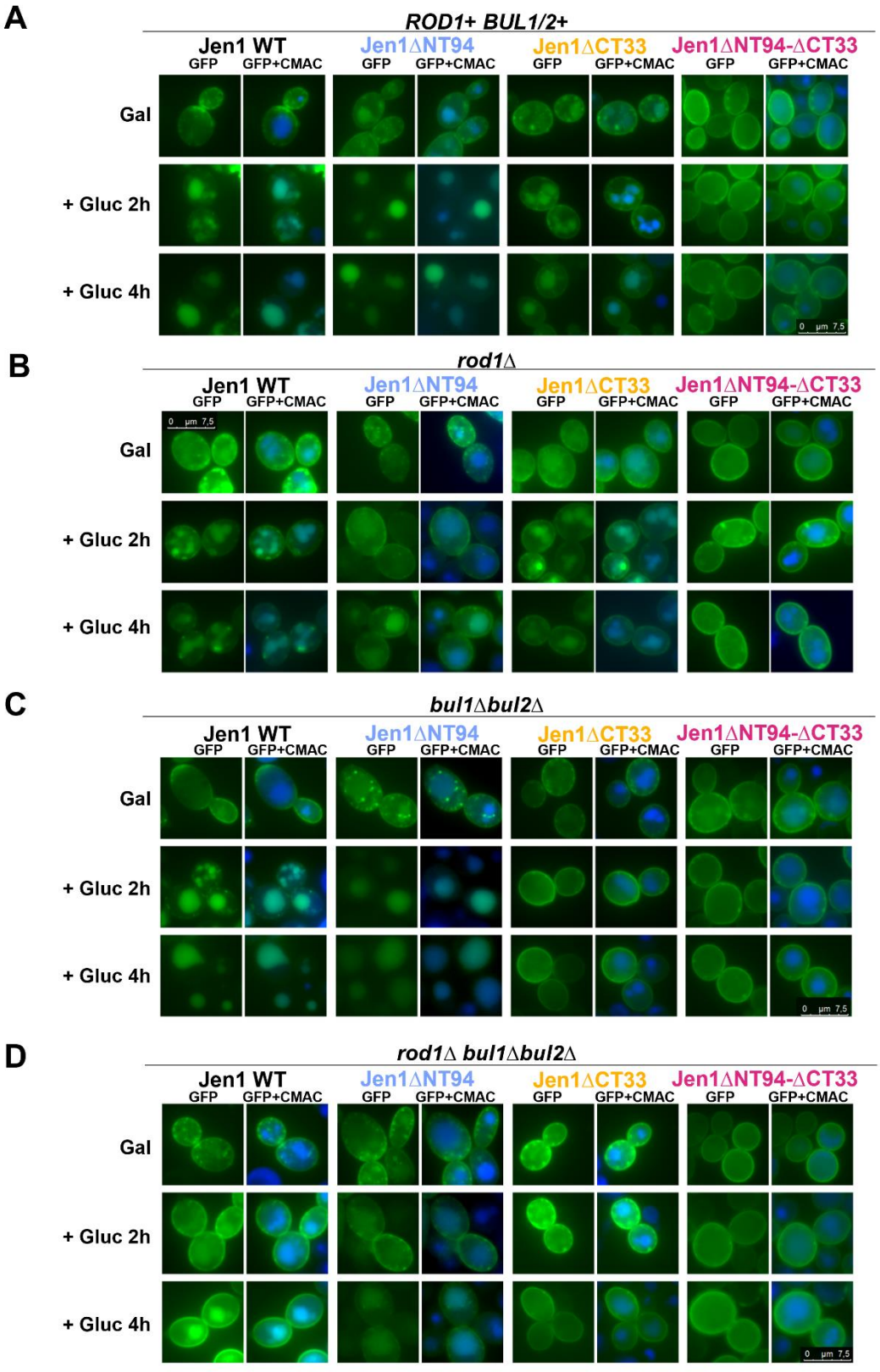

Fig. S3. Subcellular localization of Jen1 truncations in arrestin null mutants. Epifluorescence microscopy analysis of wild-type *S. cerevisiae cells* (*ROD1+ BUL1/2+*) (**A**) or of mutants lacking specific arrestins (e.g., *rod1*Δ (**B**), *bul1*Δ*bul2*Δ (**C**) or *rod1*Δ*bul1*Δ*bul2*Δ (**D**), expressing Jen1 truncations tagged with *GFP* and expressed under a *GAL* promoter. The blue CMAC dye was used as a vacuolar staining marker.

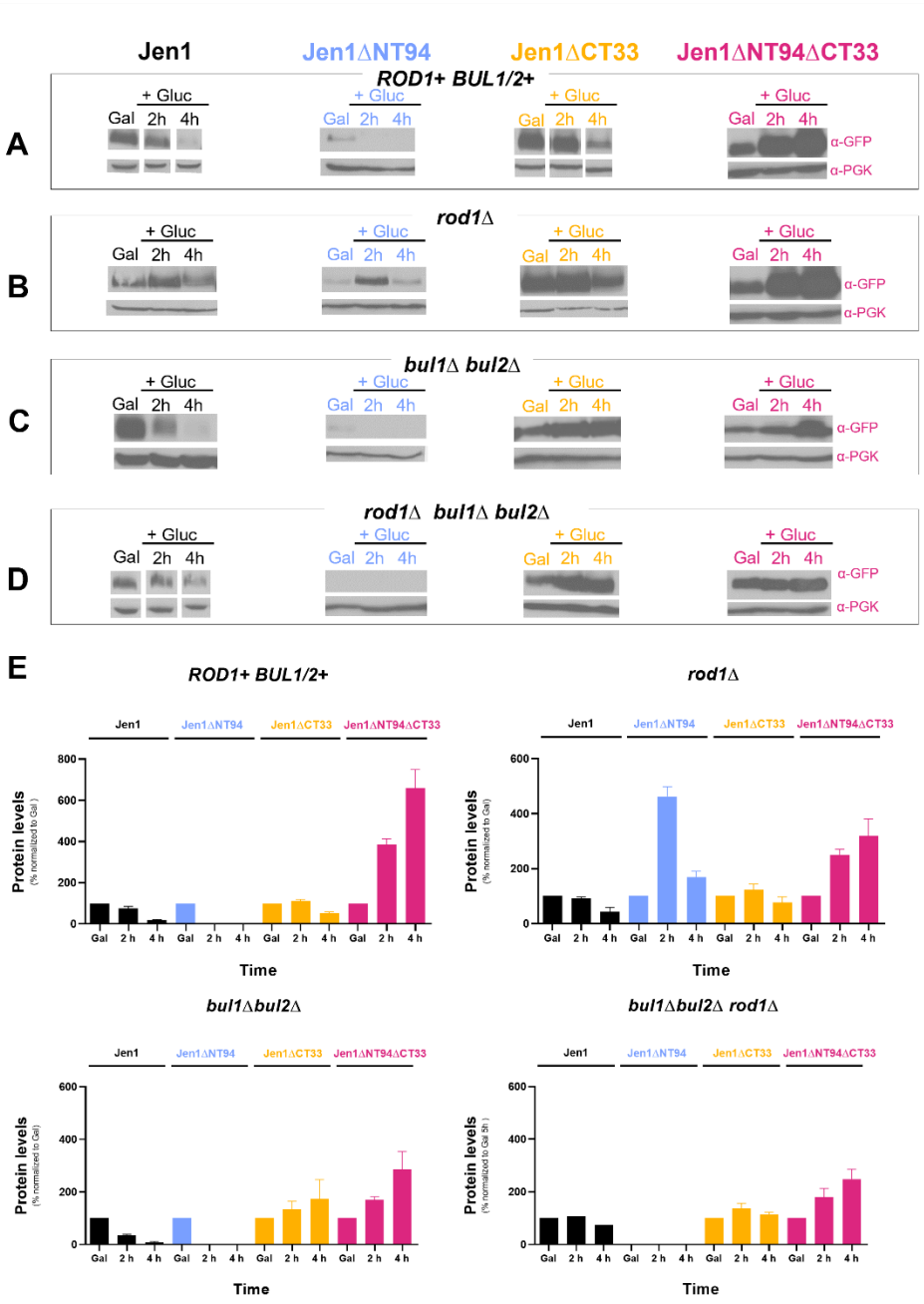

Fig. S4. Cells of *S. cerevisiae ROD1+BUL1/2+*, *rod1Δ*, *bul1Δbul2Δ* or *rod1Δbul1Δbul2Δ*, expressing the Jen1 truncations tagged with *GFP* and expressed under the *GAL1* promoter were analysed by western blot. Cells were harvested at specific time points (Gal 5 h, Gal 5 h + Gluc 2 h and Gal 5 h + Gluc 4 h), and protein extracts prepared for western immunoblotting with an anti-GFP antibody or anti-phosphoglycerate kinase (PGK) antibody (loading control) (**A-D**). **Quantification of steady state protein levels and degradation of Jen1 truncations in arrestin null mutants (E).** Relative protein levels of Jen1 wild type and Jen1 truncations expressed in a standard *S. cerevisiae* wild-type background (*ROD1+ BUL1/2+*), and in strains lacking arrestins (*rod1Δ*, *bul1Δbul2Δ* or *bul1Δbul2Δrod1Δ*). The relative quantification was carried out using ImageJ software (version 1.53k). The relative levels of protein expression of Jen1 truncations were normalized to Gal 5 h (set to 100 %). Error bars correspond to standard deviation of the mean of at least three independent experiments.

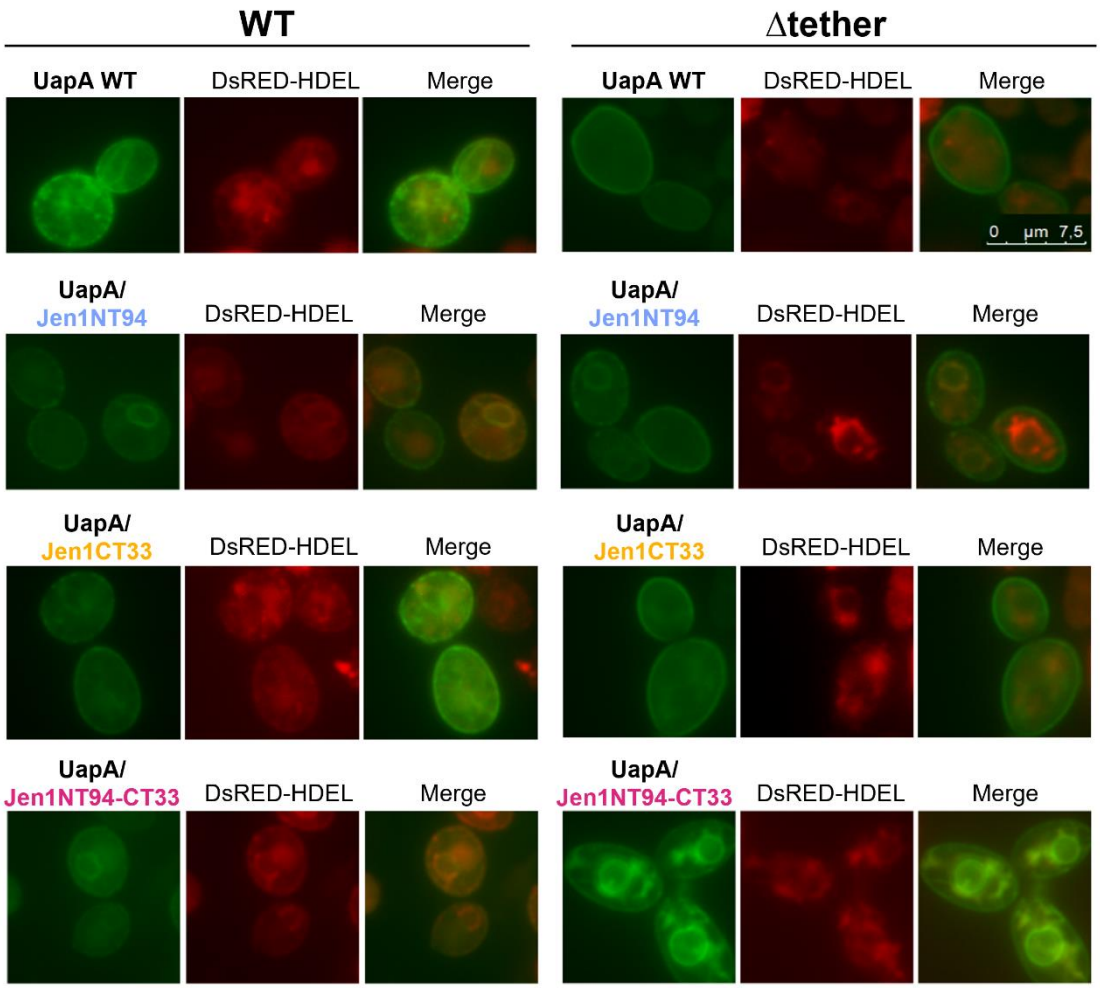

Fig. S5. Subcellular localization of UapA/Jen1 chimeras using the tether null mutant. Cells of *S. cerevisiae* lacking all tethering proteins (Δtether strain) and an isogenic wild-type control strain, expressing chimeras tagged with *GFP* and expressed under a *GAL* promoter were analyzed by epifluorescence microscopy. DsRed-HDEL was used an ER marker.

Table S2. List of the yeast strains used in this work.

Strain	Genotype	Reference/source
23344c	*MATα ura3*	B. André Collection
GT49	23344c *ura3 jen1Δ*	(Talaia et al., 2017)
GT55	23344c *ura3 rod1Δ*	(Talaia et al., 2017)
GT78	23344c *ura3 bul1Δ bul2Δ*	(Talaia et al., 2017)
GT57	23344c *ura3 bul1Δ bul2Δ rod1Δ*	B. André Collection
jen1Δ	W303-1A *leu2 ura3 trp1 his3 ade2 jen1Δ*	Sandra Paiva collection
YCS2163	SEY6210.1 *DsRed-HDEL::LEU2*	Stefan lab collection
YCS2165	ANDY198 *DsRed-HDEL::LEU2*	Stefan lab collection
SEY6210.1	*MATa leu2-3,112 ura3-52 his3-Δ 200 trp1-Δ901 lys2-801 suc2-Δ9*	(Robinson et al., 1988)
ANDY198	SEY6210.1 *ist2Δ::HISMX6 scs2Δ::TRP1 scs22Δ::HISMX6 tcb1Δ::KANMX6 tcb2Δ::KANMX6 tcb3Δ::HISMX6*	(Manford et al., 2012)

Table S3. List of primers used in this work.

Primer	Sequence
D-NTJEN1_133	GGAGAAAAAACTATATCTAGAACTAGTGGATCCatgacatggcagaattggaa
D-CTJEN1_62	TTTACTCATGTCGACAAGCTTGATATCGAATTCaacaaaaacacaagcaaatgtg
D-CTJEN1_33	GCTATGCTCTTGAACGCAATCATGCCTGCTtcgattagtgacattgttg
RCTJEN1	TTCACCTTTAGAAAATTGACCTTGAAAATATAAATTTTCCCCaacggtctcaatatg ctcct
CYC1TERM	AATGTAAGCGTGACATAACTAATTACATG
Fw_GPD_jen1dNT94	tctagaactagtggatcccccgggctgcagATGAAGCCAAACCTAAGCGC
Rev_GFP_jen1	gaggtcgacggtatcgataagcttgatatcCTAATGGTGATGGTGATGGT
GPDfwd	ATGATTACGCCAAGCGCG
GALrev	tattttctcatctgtaattgacgacgacatGGATCCACTAGTTCTAGAATCC
GPDfw_new	ATGATTACGCCAAGCGCGCAATTAA
GALrev_dNT94	ctgcagcccgggggatccactagttGGATCCACTAGTTCTAGAAT
381	acgccaagcgcgcaattaaccc
UapA_rev_33	cgtcttttgttcaacaatgtcactaatcgaAGCCTGCTTGCTCTGATACT
Jen1_fw_ct33	ggcgaggcggagtatcagagcaagcaggctTCGATTAGTGACATTGTTGA
317	AATGTAAGCGTGACATAACTAATTACATG
REV_Jen1_UapA	ggggccgtcggttgaatggatggagggatcATCCTCTTCATCTTCCTCAT
FW_UapA_Jen1	GGTGTAGAGTATGAGGAAGATGAAGAGGATgatccctccatccattcaac
Fw-YFPn	accgttGAATTCGATATCctcgagtctagaATGGTGAGCAAGGGCGAGGA
Rv-YFPn	AATGTAAGCGTGACATAACTAATTACATGAttacatgatatagacgttgt
newFw-Jen1-13	GCAGGAATTCGATATCAAGCTTATCGATACCatgtcgtcgtcaattacaga
Rv-Jen1-13	CTTGATGCCGTTCTTCTGCTTGTCGGCCATGTCGACAAGCTTGATATCGA
Fw-YFPc-13	accgttGAATTCGATATCAAGCTTGTCGACATGGCCGACAAGCAGAAGAA
newRv-YFPc-13	agcgtgacataactaattacatgactcgagTTACTTGTACAGCTCGTCCA
newFw-YnJ	CAGGAATTCGATATCAAGCTTATCGATACCatggtgagcaagggcgagga
newRv-YnJ	tattttctcatctgtaattgacgacgacatCATGATATAGACGTTGTGGC
newFw-JnYc	AACTACAACAGCCACAACGTCTATATCATGatgtcgtcgtcaattacaga
newRv-JnYc	CTTGATGCCGTTCTTCTGCTTGTCGGCCATaacggtctcaatatgctcct
newFw-YcJ	aagacatatgaggagcatattgagaccgttATGGCCGACAAGCAGAAGAA
newRv-YcJ	AGCGTGACATAACTAATTACATGACTCGAGTTACTTGTACAGCTCGTCCA
Fw-ctr-YFPn	gtttcgacggatTCTAGAACTAGTGGATCCATGGTGAGCAAGGGCGAGGA
Rv-ctr-YFPn	AGCGTGACATAACTAATTACATGACTCGAGTTACATGATATAGACGTTGT
Fw-ctr-YFPc	gtttcgacggatTCTAGAACTAGTGGATCCATGGCCGACAAGCAGAAGAA
Rv-ctr-YFPc	AGCGTGACATAACTAATTACATGACTCGAGTTACTTGTACAGCTCGTCCA
Fw_Jen1MidSeq	Gagttttcttgggagaatgtc

Rev_p416_seq	GGTTGTCTAACTCCTTCCT
RevSeqJen1Mid	TCCCTAAAGTAGCCAAAGGCTCTGT
GPDFWD	ACGCCAAGCGCGCAATTAACCC
GPDREV	catGGATCCACTAGTTCTAGatccgtcgaaactaagtt
Fw-CT33-UapA	CGTCAAGGAGAAAAAACCCCGGATTCTAGAatgtcgattagtgacattgt
Rev-CT33-UapA	Gccgtcggttgaatggatggagggatcaacggtctcaatatgctcctc

Table S4. List of plasmids used in this work.

Plasmid name	Description	Source/reference
pGALJEN1	*URA3, GAL::JEN1::GFP*	(Paiva et al., 2009)
p416GPD	*URA3, GPD*	(Mumberg et al., 1995)
p413GPD	*HIS3, GPD*	(Mumberg et al., 1995)
p426GPD	*URA3, GPD*	(Mumberg et al., 1995)
pGPDJEN1	*URA3, GPD::JEN1::GFP*	This study
pGPDJEN1ΔNT133	*URA3, GPD::JEN1ΔNT133::GFP*	This study
pGPDJEN1ΔNT94	*URA3, GPD::JEN1ΔNT94::GFP*	This study
pGPDJEN1ΔCT62	*URA3, GPD::JEN1ΔCT62::GFP*	This study
pGPDJEN1ΔCT33	*URA3, GPD::JEN1ΔCT33::GFP*	This study
pGPDJEN1ΔNT94-ΔCT33	*URA3, GPD::JEN1ΔNT94:: JEN1ΔCT33::GFP*	This study
pGALJEN1ΔNT94	*URA3, GAL::JEN1ΔNT94::GFP*	This study
pGALJEN1ΔCT33	*URA3, GAL::JEN1ΔCT33::GFP*	This study
pGALJEN1ΔNT94-ΔCT33	*URA3, GAL::JEN1ΔNT94::JEN1ΔCT33::GFP*	This study
PVD7	*ALCA(P)::YFPN::APSB1.5*	(Zekert et al., 2010)
PVD8	*ALCA(P)::YFPC::APSB1.5*	(Zekert et al., 2010)
pGPDJEN1YFP$_N$	*URA3, GPD::JEN1::YFP$_N$*	This study
pGPDJEN1YFP$_C$	*HIS3, GPD::JEN1::YFP$_C$*	This study
pGPDYFP$_N$JEN1YFP$_C$	*URA3, GPD:: YFP$_N$::JEN1::YFP$_C$*	This study
pGPDYFP$_N$	*URA3, GPD::YFP$_N$*	This study
pGPDYFP$_C$	*URA3, GPD::YFP$_C$*	This study
pDDGFP2UAPA	*URA3, GAL::UAPA::GFP*	(Leung et al., 2010)
pDDGFP2-UapAΔCT/Jen1CT62	*URA3, GAL::UAPAΔCT/JEN1CT62::GFP*	This study
pGALUAPA/JEN1NT94	*URA3, GAL JEN1NT94::UAPA::GFP*	This study
pGALUAPA/JEN1CT33	*URA3, GAL::UAPA::JEN1CT33::GFP*	This study
pGALUAPA/JEN1NT94-CT33	*URA3, GALJEN1NT94::UAPA::JEN1CT33::GFP*	This study
pGALJEN1CT33/UAPA	*URA3, GAL::JEN1CT33::UAPA:: GFP*	This study

References

Bernsel, A., Viklund, H., Hennerdal, A. and Elofsson, A. (2009). TOPCONS: Consensus prediction of membrane protein topology. *Nucleic Acids Res.* **37**, 465–468.

Leung, J., Karachaliou, M., Alves, C., Diallinas, G. and Byrne, B. (2010). Expression and purification of a functional uric acid-xanthine transporter (UapA). *Protein Expr. Purif.* **72**, 139–46.

Manford, A. G., Stefan, C. J., Yuan, H. L., MacGurn, J. A. and Emr, S. D. (2012). ER-to-Plasma Membrane Tethering Proteins Regulate Cell Signaling and ER Morphology. *Dev. Cell* **23**, 1129–1140.

Mumberg, D., Müller, R. and Funk, M. (1995). Yeast vectors for the controlled expression of heterologous proteins in different genetic backgrounds. *Gene* **156**, 119–22.

Paiva, S., Vieira, N., Nondier, I., Haguenauer-Tsapis, R., Casal, M. and Urban-Grimal, D. (2009). Glucose-induced ubiquitylation and endocytosis of the yeast Jen1 transporter. Role of lysine 63-linked ubiquitin chains. *J. Biol. Chem.* **284**, 19228–19236.

Robinson, J. S., Klionsky, D. J., Banta, L. M. and Emr, S. D. (1988). Protein sorting in Saccharomyces cerevisiae: isolation of mutants defective in the delivery and processing of multiple vacuolar hydrolases. *Mol. Cell. Biol.* **8**, 4936–4948.

Talaia, G., Gournas, C., Saliba, E., Barata-Antunes, C., Casal, M., André, B., Diallinas, G. and Paiva, S. (2017). The α-Arrestin Bul1p Mediates Lactate Transporter Endocytosis in Response to Alkalinization and Distinct Physiological Signals. *J. Mol. Biol.* **429**, 3678–3695.

Zekert, N., Veith, D. and Fischer, R. (2010). Interaction of the Aspergillus nidulans microtubule-organizing center (MTOC) component ApsB with gamma-tubulin and evidence for a role of a subclass of peroxisomes in the formation of septal MTOCs. *Eukaryot. Cell* **9**, 795–805.

Zimmermann, L., Stephens, A., Nam, S.-Z., Rau, D., Kübler, J., Lozajic, M., Gabler, F., Söding, J., Lupas, A. N. and Alva, V. (2018). A Completely Reimplemented MPI Bioinformatics Toolkit with a New HHpred Server at its Core. *J. Mol. Biol.* **430**, 2237–2243.